Studies on Stem Cell Biology Using a Fluorescent Ubiquitination-based Cell Cycle Indicator

A Dissertation Submitted to
the Graduate School of Life and Environmental Sciences,
the University of Tsukuba
in Partial Fulfillment of the Requirements
for the Degree of Doctor of Philosophy in Science
(Doctoral Program in Biological Sciences)

Masahiro YO

Contents

Abstract

Stem cells are undifferentiated cells capable of both self-renewal and multi-lineage differentiation. There are two types of stem cells: pluripotent stem cells (PSCs) and adult stem cells. PSCs, such as embryonic stem cells (ESCs) and induced pluripotent stem cells (iPSCs), can generate any cell types of the body. In contrast, adult stem cells have restricted potential to differentiate into certain organ or tissue types. For example, hematopoietic stem cells (HSCs) are defined as primitive cells that have the ability to self-renew and differentiate into all types of blood cells.

The regulation of stem cell proliferation and differentiation is essential for the accurate morphogenesis and maintenance of tissue integrity. Recent studies suggest that the unique cell cycle properties of stem cells are functionally important for maintaining multipotency. However, molecular mechanisms regulating the cell cycle of stem cells are still far from being fully understood partly because of the lack of accurate methods for determining and tracking the cell cycle status of individual living cells.

Fluorescent ubiquitination-based cell cycle indicator (Fucci) technology utilizing the cell cycle-dependent proteolysis of ubiquitin oscillators enables visualization of cell cycle progression in individual living cells. The Fucci probe consists of two chimeric fluorescent proteins, FucciS/G_2/M and FucciG_1, which label the nuclei of cells in S/G_2/M phase green and those in G_1 phase red, respectively. Fucci technology allows us to analyze the spatial and temporal patterns of cell cycle dynamics in vitro and in vivo.

In chapter I, I aimed to investigate cell cycle status of intravital HSCs. I generated transgenic mice expressing Fucci probes and analyzed transgene expression in hematopoietic cells using flow cytometry. The FucciS/G_2/M-#474 and FucciG_1-#639 mouse lines exhibited high-level transgene expression in most hematopoietic cell populations. The FucciG_1-#610 line expressed the transgene at high levels predominantly in the HSC (CD34$^-$KSL: CD34$^{-/low}$c-Kit$^+$Sca-1$^+$lineage marker$^-$) population. Analysis of the HSC population in the transgenic mice expressing both FucciS/G_2/M and FucciG_1 (#474/#610) confirmed that more than 95% of the cells were in G_0/G_1 phase, although the FucciG_1(red) intensity was heterogeneous. An in vivo competitive repopulation assay revealed that repopulating activity resided largely in the FucciG_1(red)^{high} fraction of CD34$^-$KSL cells. Thus, the CD34$^-$KSL HSC population can be further purified on the basis of the Fucci intensity.

In chapter II, I investigated the cell cycle of PSCs. PSCs are classified into two distinct pluripotent states: naïve and primed. Naïve and primed PSCs differ in colony

morphology, X chromosome inactivation pattern, and requirement of signaling pathways for in vitro self-renewal. Most importantly, both naïve and primed PSCs have the ability to form teratomas but only naïve PSCs readily contribute to chimera formation after blastocyst injection. Thus, primed PSCs represent a more differentiated state than naïve PSCs. PSCs have a peculiar cell cycle, which is thought to be involved in pluripotency and maintaining undifferentiated state. Therefore, I introduced Fucci probes into naïve and primed PSCs using lentiviral vectors and investigated the spatio-temporal patterns of cell cycle dynamics in PSCs. A significant number of cells with prolonged G_1 phase were observed in primed PSCs and the mean length of the G_1 phase of primed and naïve-like PSCs was longer than that of naïve PSCs, suggesting that prolonged G_1 phase is closely related to the state of PSCs. The prolonged G_1 phase is probably due to contact inhibition. The G_1 phase length had no affect on the length of each cell cycle phase in sequential cell division.

In this study, cell cycle analysis in individual living stem cells using Fucci technology revealed heterogeneity in stem cell population, which is involved in stem cell function.

General Introduction

Stem cells are undifferentiated cells capable of both self-renewal and multi-lineage differentiation. Stem cell research is a promising field with attractive applications, such as regenerative medicine and drug discovery (Ramakrishna et al., 2011). Stem cells can be categorized into two types: pluripotent stem cells (PSCs) and adult stem cells.

Pluripotent stem cells and adult stem cells

Pluripotent stem cells (PSCs) can differentiate into all cell types derived from the three embryonic germ layers. Embryonic stem cells (ESCs) and induced pluripotent stem cells (iPSCs) are well-known PSCs. ESCs are derived from the inner cell mass of pre-implantation blastocysts (Evans et al., 1981; Thomson et al., 1988). Although ESCs are expected to be exploited in regenerative medicine, use of human ESCs (hESCs) has the ethical concerns and the risk of immune rejection after transplantation. Fortunately, the problem was resolved by the generation of human iPSCs (hiPSCs) from somatic cells by introducing four transcription factors, Oct4, Sox2, Klf4, and c-Myc (Takahashi et al., 2007). A number of ways to generate and culture hiPSCs have been reported to improve safety and efficiency aimed at clinical application (Yamanaka, 2012), but another difficulty arises from pluripotent state.

PSCs can be classified into two distinct pluripotent states: naïve and primed (Nichols et al., 2009). Mouse ESCs (mESCs) and iPSCs (miPSCs) represent naïve PSCs, which are characterized by compact and domed colony morphology, global reduction in DNA methylation, and two active X chromosomes in female. In addition, mESCs/iPSCs require external factors leukemia inhibitory factor (LIF) and bone morphogenetic protein 4 (BMP4) signaling for in vitro self-renewal (Smith et al., 1988; Ying et al., 2003). BMP4 can be replaced by small molecules, MEK inhibitor and GSK3 inhibitor (Olariu et al., 2013). Most importantly, mESCs/iPSCs can efficiently contribute to cell types of the body including the germline after blastocyst injection.

On the other hand, mouse epiblast stem cells (mEpiSCs) derived from the post-implantation epiblasts represent primed PSCs (Borns et al., 2007). mEpiSCs display flattened monolayer colony morphology, increase in DNA methylation, X chromosome inactivation in female, and dependence on basic fibroblast growth factor (bFGF) and Activin/Nodal signaling for pluripotency and self-renewal. mEpiSCs express only some of the pluripotency factors: Oct4, Sox2, and Nanog are highly expressed, while Klf4 are expressed in low levels (Silva et al., 2009; Guo et al., 2009). Although

mEpiSCs have the ability to form teratomas, they rarely contribute to chimera formation after blastocyst injection (Nichols et al., 2009). Unlike mouse PSCs, ESCs/iPSCs derived from other species, including humans, rabbits, pigs, and primates, are in the primed state. Recent studies have shown that primed PSCs can be converted to the naïve-like state that have properties of naïve PSCs expect for the ability to contribute to chimeras (Hanna et al., 2010; Honda et al., 2013; Fujishiro et al., 2013; Gafni et al., 2013; Theunissen et al., 2014; Takashima et al., 2014).

In contrast to PSCs, adult stem cells can differentiate into only several lineages. For example, hematopoietic stem cells (HSCs) have the ability to self-renew and differentiate into all blood cell types (Kondo et al., 2003). HSC transplantation is used to treat leukemia and other blood diseases (Shizuru et al., 2005). In this context, ex vivo expansion of HSCs would have widespread clinical applications including gene therapy. However, the methods for amplification of HSCs without loss of stem cell activity or isolation of HSCs with absolute purity have not been achieved.

Cell cycle of pluripotent stem cells

PSCs have unique cell cycle properties characterized by a rapid proliferation with a very short G_1 phase (Savatier et al., 1994; White et al., 2005). In general, proliferation of somatic cells is responsive to exogenous growth factors. In the absence of these signals, somatic cells arrest in G_1 phase or enter into quiescent G_0 phase. However, PSCs are less reliant on exogenous growth factors and are not subject to contact inhibition (Savatier et al., 1994; Schratt et al., 2001; Stead et al., 2002). This may be owing to an autocrine loop of PSC growth factor signaling, or a cell autonomous mode of cell division that does not require such signaling cascades. It has been shown that, unlike somatic cells, constitutive Cdk activities in mESCs lead to an inactivation of Rb family members, resulting in cell cycle-independent activation of E2F target genes (White et al., 2005). Other factors such as miRNAs have also been reported to be involved in cell cycle regulation of PSCs (Abdelalim, 2013). It has been hypothesized that rapid proliferation of PSCs with the shortened G1 is essential for self-renewal and pluripotency (Izpisua et al., 2011; Markossian et al., 2013; Calder et al., 2013).

Cell cycle of hematopoietic stem cells

The cell cycle of adult stem cells is regulated appropriately. HSCs rapidly generate progenitor cells and blood cells during fetal life: more than 95% of HSCs are actively cycling in the mouse fetal liver with a cell cycle transit time between 10–14 hours (Bowie et al., 2006; Nygren et al., 2006). However, in the adult bone marrow (BM),

HSC population rapidly switches to a quiescent state by four weeks of age, with only 5% of total HSCs actively in the cell cycle thereafter through adult life (Cheshier et al., 1999; Bowie et al., 2006; Kiel et al., 2007). The balance between HSC quiescence and proliferation is thought to be strictly regulated by a complex network of cell-intrinsic and cell-extrinsic factors in a specific microenvironment, referred to as the niche (Pietras et al., 2011). However, the mechanisms controlling cell cycle activity of HSCs are still largely unknown.

Cell cycle analysis and Fucci technology

The relationship between regulation of cell cycle and potency of stem cells has been investigated. However, until recently, cell cycle analysis has been conducted mainly by using cell cycle markers or flow cytometry (Nunez et al., 2001; Whitfield et al., 2006). Detection of markers used in cell cycle studies usually needs the staining, and some of them also need the fixation of the cells. Those markers are not suitable for intravital cells and long term monitoring of cell cycle. Similarly, flow cytometry can only investigate the proportion of each cell cycle phase. Therefore, molecular mechanisms regulating the cell cycle of stem cells are still far from being fully understood partly because of the lack of accurate methods for determining and tracking the cell cycle status of individual living cells.

Currently, these limits are overcome by the development of fluorescent ubiquitination-based cell cycle indicator (Fucci) technology (Sakaue-Sawano et al., 2008). Fucci technology relies on the precisely regulated cell cycle-dependent proteolysis of two factors, Geminin and Cdt1, which ensure that replication occurs only once during a cell cycle (Askew et al., 2008). Cdt1 and Geminin are controlled by ubiquitin-mediated proteolysis, SCF^{skp2} and APC^{Cdh1}, respectively, displaying mutual antagonism and hence reciprocal cell cycle regulated activity (Wei et al., 2004; Benmaamar et al., 2005). Cdt1 protein accumulates during G_1 but ubiquitinated for subsequent degradation by the SCF^{skp2} complex at the onset of S phase and thus absent throughout $S/G_2/M$ (Carlier et al., 2014). On the other hand, Geminin accumulates during S and G_2, but targeted for ubiquitin-mediated proteolysis by the APC^{Cdh1} complex when cell exit mitosis and G_1 phase (Carlier et al., 2014). FucciG1 probe is a fusion protein of a fragment of human Cdt1 with the red fluorescent that indicates the G1 phase. FucciS/G2/M probe is a fusion protein of a fragment of human Geminin with the green fluorescent protein that visualizes S, G2 and M phases (Sakaue-Sawano et al., 2008). Generating stable cell lines and transgenic mice that constitutively express Fucci probes allows us to analyze the spatio-temporal patterns of cell cycle dynamics (Sakaue-Sawano et al., 2013).

By taking advantage of Fucci technology, this study aimed to investigate the cell cycle of stem cells. In chapter I, I investigated cell cycle status of intravital HSCs using transgenic mice expressing Fucci probes. In chapter II, I introduced Fucci probes into PSCs using lentiviral vectors and investigated the spatio-temporal patterns of cell cycle dynamics in PSCs.

Chapter I

Generation and characterization of transgenic mice expressing Fucci probes for cell cycle analysis of hematopoietic cells

Introduction

Hematopoiesis is a hierarchical differentiation process by which all blood cell types are generated from hematopoietic stem cells (HSCs). HSCs are capable of self-renewal and multilineage differentiation. In the adult bone marrow (BM), HSCs are predominantly quiescent and reside in a specific microenvironment, referred to as the niche, where HSC quiescence, self-renewal, proliferation, and differentiation are thought to be strictly regulated in order to maintain the HSC pool and sustain lifelong production of blood cells (Morrison SJ et al., 2014). HSCs give rise to highly proliferative progenitors with limited or no self-renewal capacity and lineage-restricted differentiation potential, producing terminally differentiated hematopoietic cells. Cell cycle regulation plays a critical role in hematopoiesis (Pietras EM et al., 2011). Although many intrinsic and extrinsic factors are involved in hematopoiesis, the regulatory mechanisms underlying hematopoietic cell proliferation and differentiation are still unclear. Visualizing the progress of the cell cycle in hematopoietic cells including HSCs will provide valuable information for better understanding how cell cycle progression and hematopoiesis are coordinated.

Fluorescent ubiquitination-based cell cycle indicator (Fucci) technology makes it possible to visualize cell cycle progression in living cells (Sakaue-Sawano et al., 2008). This technology utilizes the cell cycle-dependent proteolysis of two ubiquitin oscillators, human Cdt1 and geminin. The original Fucci probe was generated by fusing monomeric Kusabira Orange 2 (mKO2) and monomeric Azami Green (mAG) to the ubiquitination domains of Cdt1 (hCdt1(30/120)) and geminin (hGem(1/110)), respectively. The resulting mKO2-hCdt1(30/120) and mAG-hGem(1/110) fusion proteins label the nuclei of cells in G_1 phase red and those in $S/G_2/M$ phase green, respectively. Using Fucci probes, the cell cycle behavior of individual cells was visualized in vitro and in vivo (Hama H et al., 2011; Ge WP et al., 2012; Juuri E et al., 2012; Sakaue-Sawano et al., 213).

In this study, transgenic mice expressing Fucci probes were generated and I analyzed transgene expression in hematopoietic cells including HSCs. I also analyzed the relationship between Fucci signal intensity and repopulating activity of HSCs.

Materials and methods

Fucci transgenic mice

Generation of Fucci transgenic mice expressing mAG-hGem(1/110) and mKO2-hCdt1(30/120) under the control of the CAG promoter has been reported previously (Sakaue-Sawano A et al., 2008). Transgenic mouse lines (FucciS/G_2/M-#474, -#492, -#504 and FucciG_1-#596, -#610, -#639) were backcrossed to C57BL/6N (B6-Ly5.2) mice for more than ten generations and can be obtained from RIKEN BioResource Center (Tsukuba, Japan). All animal experiments were approved by the Animal Experiment Committee at the RIKEN Tsukuba Institute.

Analysis of transgene expression

Hematopoietic cells were isolated from BM, peripheral blood (PB), spleen, and thymus of Fucci transgenic mice (3-6 months of age). The cells were stained with cell surface marker antibodies. The following antibodies were used: APC-, APC-Cy7-, PE-Cy7, or PerCP-Cy5.5-conjugated anti-B220, anti-CD3, anti-CD4, anti-CD8, anti-NK1.1, anti-Gr-1, anti-Mac-1, anti-CD41, anti-Ter119, anti-c-Kit, anti-Sca-1, anti-Fc γ R, anti-IL-7Ra, and anti-CD34 (all antibodies purchased from eBioscience, San Diego, CA). Lineage marker (Lin) antibodies consist of biotinylated anti-Gr-1, anti-Mac-1, anti-B220, anti-IgM, anti-CD4, anti-CD8, and anti-Ter119. The biotinylated antibodies were developed with APC-Cy7-conjugated streptavidin (eBioscience). Fluorescence-activated cell sorting (FACS) analysis was performed with a FACSCalibur or a FACSAriaIII equipped with four lasers (405, 488, 561, and 633 nm) (BD Biosciences, San Jose, CA).

Competitive repopulation assay

B6-Ly5.2 mice were purchased from Charles River Laboratories Japan. B6-Ly5.1 mice were obtained from RIKEN BioResource Center. B6-Ly5.1/Ly5.2 F1 mice were obtained by mating pairs of B6-Ly5.1 and B6-Ly5.2 mice. BM cells isolated from Fucci transgenic mice (B6-Ly5.2) were stained with biotinylated Lin antibodies. The cells were then stained with eFluor660-conjugated anti-CD34, PE-Cy5.5-conjugated anti-Sca-1, and PE-Cy7-conjugated anti-c-Kit antibodies (eBioscience). The biotinylated antibodies were developed with APC-eFluor780-conjugated streptavidin (eBioscience). Twenty FACS-sorted FucciG_1(red fluorescence)^{high} or FucciG_1(red fluorescence)^{low} CD34$^{-/low}$c-Kit$^+$Sca-1$^+$Lin$^-$ (CD34$^-$KSL) cells were mixed with 2×10^5 total BM competitor cells from B6-Ly5.1/5.2 F1 mice and transplanted into lethally (9.5 Gy)

irradiated B6-Ly5.1 mice. At various time points after transplantation, PB cells of the recipient mice were collected and stained with biotinylated anti-Ly5.2 (BD Biosciences), APC-conjugated anti-Ly5.1, PE-Cy7-conjugated anti-Mac-1, PE-Cy7-conjugated anti-Gr-1, PE-Cy7-conjugated anti-B220, eFluor450-conjugated anti-CD4, and eFluor450-conjugated anti-CD8 antibodies (eBioscience). The biotinylated antibody was developed with APC-eFluor780-conjugated streptavidin. FACS analysis was performed with a FACSAriaIII. Donor chimerism was determined as the percentage of $Ly5.2^+$ cells.

Results

Analysis of transgene expression in hematopoietic cells of Fucci transgenic mice

Generation of eight transgenic mice expressing mAG-hGem(1/110) (FucciS/G_2/M) and 16 transgenic mice expressing mKO2-hCdt1(30/120) (FucciG_1) has been reported previously (Sakaue-Sawano A et al., 2008). Analysis of whole body sections from newborn mice revealed high-level transgene expression in FucciS/G_2/M transgenic mouse lines (#474, #492, #504, and #514) and FucciG_1 lines (#596, #610, #639, and #659). Then, these eight mouse lines were further analyzed by FACS for the transgene expression in various hematopoietic cell populations of BM cells (Figure 1-1). The Fucci transgenes were expected to be highly expressed apparently in all tissues of the FucciS/G_2/M-#504 and FucciG_1-#596 lines (Sakaue-Sawano A et al., 2008). However, the FACS data indicated that these two lines and FucciG_1-#659 line expressed transgenes at very low levels in all hematopoietic cell populations we analyzed.

FucciS/G_2/M-#474 had the highest transgene expression in most hematopoietic cell populations. Note that high-level transgene expression was observed preferentially in B lymphoid cells from FucciS/G_2/M-#492 mice. FucciS/G_2/M-#492 was successfully used to visualize the localization of activated proliferating memory B cells in the spleen (Aiba Y et al., 2010). FucciG_1-#610 and FucciG_1-#639 expressed the transgene at high levels, especially in HSCs ($CD48^-$KSL or $CD34^-$KSL) and mature hematopoietic cell populations, respectively.

Next, I generated transgenic mice expressing both FucciS/G_2/M and FucciG_1 by cross-breeding FucciS/G_2/M-#474 with FucciG_1-#610, and analyzed transgene expression in cells from various hematopoietic organs. As shown in Figure 1-2, transgene expression was detected in mature hematopoietic cell populations from the PB, BM, spleen, and thymus. As expected, the number of FucciG_1(red)-positive cells increased with differentiation from immature to mature cells (e.g., immature $CD4^+CD8^+$ T cells vs. mature $CD4^+CD8^-$ or $CD4^-CD8^+$ T cells in the thymus). On the other hand, the number of FucciS/G_2/M(green)-positive cells increased with the differentiation of HSCs into multipotent progenitors (MPPs) and lineage-restricted progenitors, common lymphoid progenitors (CLPs), common myeloid progenitors (CMPs), granulocyte/macrophage progenitors (GMPs), and megakaryocyte/erythrocyte progenitors (MEPs).

3.2. Analysis of Fucci fluorescence intensity and repopulating activity of HSCs

Next, I analyzed the HSC population of #474/#610 mice in detail. More than 95% of $CD34^-KSL$ cells were $FucciG_1(red)$-positive (Fig. 1-3a), confirming that HSCs are predominantly in G_0/G_1 phase. Interestingly, heterogeneous fluorescence intensities were found in the $FucciG_1(red)$-positive population. The proportion of $FucciG_1(red)^{high}$ cells was significantly higher in the HSC ($CD34^-KSL$) population than in the MPP ($CD34^+KSL$) population. This finding suggests that $FucciG_1(red)^{high}$ cells are in more quiescent or stay longer in G_0/G_1 phase than $FucciG_1(red)^{low}$ cells. The $FucciG_1(red)$ intensity was also heterogeneous in other HSC populations using CD150 and CD48 markers (Kiel MJ et al., 2005) (Supplementary Fig. 1-5), although these HSC populations substantially overlap with each other (Ema H et al., 2006; Morita Y et al., 2013; Mayle A et al., 2013).

To assess whether $FucciG_1$ expression status correlates with repopulating activity, the $FucciG_1(red)^{high}$ or $FucciG_1(red)^{low}$ fraction of $CD34^-KSL$ cells was sorted by FACS (Fig. 1-3b) and subjected to an in vivo competitive repopulation assay. As shown in Figure 1-3c, repopulating activity was found to reside mainly in the $FucciG_1(red)^{high}$ cell population. I also cultured $FucciG_1(red)^{high}$ and $FucciG_1(red)^{low}$ $CD34^-KSL$ cells in vitro with a combination of cytokines (stem cell factor, thrombopoietin, fibroblast growth factor-1, and insulin-like growth factor-2) (Noda S et al., 2008). No significant differences were found in the timing of the first cell division and the duration of the cell cycle between these two cell populations (data not shown). The cell cycle state of $CD34^-KSL$ cells appears to not influence the induction of cell proliferation under the in vitro culture conditions.

Discussion

I generated Fucci transgenic mouse line #474/#610 expressing both FucciS/G_2/M and FucciG_1 in various hematopoietic cells, especially HSCs. Thus, #474/#610 mice are useful for studying the cell cycle dynamics of HSC differentiation into mature hematopoietic cells. Using #474/#610 mice, we were able to visualize endomitosis in megakaryoblasts differentiated from HSCs, MPPs, CMPs, and MEPs (Sakaue-Sawano A et al., 2013). It would be interesting to analyze hematopoietic cell cycle dynamics in mice generated by crossing #474/#610 mice with mutant mice associated with hematopoietic abnormalities in future studies.

It is generally accepted that HSCs in the adult BM are almost exclusively in quiescent G_0 phase. The results with Fucci probe also suggest that most HSCs remain in G_0/G_1 phase. FucciG_1(red)^{high} cells in HSC populations appear to be in G_0 phase for a long period of time, but the Fucci probe used in this study cannot distinguish between G_0 and G_1 phase. Recently, a fusion protein of the fluorescent protein mVenus and a p27K$^-$ mutant lacking CDK inhibitory activity (mVenus-p27K$^-$) was shown to be capable of visualizing cells in G_0 phase (Oki T et al., 2014). In combination with Fucci probe, mVenus-p27K$^-$ probe is also capable of distinguishing between cells in G_0 phase and cells in G_1 phase during the G_0–G_1 transition. Therefore, the relationship between FucciG_1(red) intensity and duration of G_0 phase in HSC populations could be analyzed using mVenus-p27K$^-$ probe. Unfortunately, the expression of mVenus-p27K$^-$ was reported to be low or undetectable in hematopoietic cells from mVenus-p27K$^-$ transgenic mice. However, time-lapse analysis of HSC division in the BM niche of mice transplanted with HSCs expressing Fucci and mVenus-p27K$^-$ probes, if possible (Celso CL et al., 2009; Xie Y et al., 2009; Kohler A et al., 2009), will provide valuable information about HSC biology.

Purification of HSCs is important when studying their self-renewal and differentiation, especially at a clonal level. Substantial progress has been made in isolating murine HSCs using a combination of cell surface markers and flow cytometry. CD34$^-$KSL cells are highly purified HSCs. However, single-cell transplantation studies identified only 20–40% of CD34$^-$KSL cells as long-term repopulating cells (Ema H et al., 2006; Noda S et al., 2008; Osawa M et al., 1996; Ema H et al., 2000; Takano H et al., 2004). Because the seeding efficiency is thought to be more than 50% (Ema H et al., 2006), CD34$^-$KSL cells are still not a pure population of HSCs. In the present study, we demonstrated that the fluorescence intensity of FucciG_1(red) can be used for further purification of CD34$^-$KSL HSCs, and probably other HSC populations such as

CD150^{+}CD48^{-}KSL and CD34^{-}CD150^{+}KSL cells. Adult HSC-specific properties, including cell cycle quiescence, are altered during ontogeny and aging (Pietras EM et al., 2011; Boisset JC et al., 2012; Geiger H et al., 2013). In addition, recent studies have identified functionally distinct HSC subtypes, including myeloid-biased, lymphoid-biased, and balanced HSCs (Copley MR et al., 2012). Thus, Fucci transgenic mice are expected to facilitate further characterization of HSCs with distinct properties in terms of their cell cycle status.

Chapter II

Cell cycle analysis of pluripotent stem cells using Fucci probes

Introduction

Pluripotent stem cells (PSCs) have the ability to self-renew and differentiate into all cell types of the body. PSCs can be classified into two distinct pluripotent states: naïve and primed (Nichols et al., 2009) (Fig. 2-1).

Mouse embryonic stem cells (mESCs) (Evans et al., 1981) and induced pluripotent stem cells (miPSCs) (Takahashi et al., 2006) represent naïve PSCs, which are characterized by compact and domed colony morphology, global reduction in DNA methylation, two active X chromosomes in female, and requirement of leukemia inhibitory factor (LIF) and bone morphogenetic protein 4 (BMP4) signaling pathways for in vitro self-renewal (Smith et al., 1988; Ying et al., 2003). In addition, mESCs/iPSCs can efficiently contribute to cell types of the body including the germline after blastocyst injection.

On the other hand, mouse epiblast stem cells (mEpiSCs) derived from the post-implantation epiblasts represent primed PSCs (Borns et al., 2007). mEpiSCs display flattened monolayer colony morphology, increase in DNA methylation, X chromosome inactivation in female, and dependence on basic fibroblast growth factor (bFGF) and Activin/Nodal signaling for pluripotency and self-renewal. Although mEpiSCs have the ability to differentiate into cells of all three germ layers in vitro and give rise to differentiated teratomas, they rarely contribute to chimera formation after blastocyst injection (Nichols et al., 2009). Unlike mouse PSCs, ESCs/iPSCs derived from other species, including humans, rabbits, pigs, and primates, are classified as the primed state.

Recent studies have shown that primed PSCs can be converted to the naïve-like state by expressing exogenous genes and/or cultivation with small molecules and cytokines (Hanna et al., 2010; Honda et al., 2013; Fujishiro et al., 2013; Gafni et al., 2013; Theunissen et al., 2014; Takashima et al., 2014). These naive-like PSCs exhibit the naive state properties, but they have a limited capacity for producing chimeric offspring. Because it is not allowed to produce human chimeras, appropriate markers are required to evaluate the state of human PSCs in vitro.

PSCs have unique cell cycle features. Cultured mESCs exhibit a high rate of proliferation and a short cell cycle time (10-12 hours) (Stead et al., 2002). Similarly, hESCs and hiPSCs have a short G1 phase (2-3 hours) and an abbreviated cell cycle (16-18 hours) (Becker et al., 2006; Fluckiger et al., 2006; Ghule et al., 2011). A short G_1 phase is a characteristic of the PSCs (Ruiz et al., 2011). This short G_1 phase is associated with a unique mechanism of cell cycle regulation (Suvorova et al., 2012).

Generally, cell fate is determined during G1 phase the mammalian cell cycle (Blomen et al., 2007; Pfeuty et al., 2008). Recent studies suggest that a short G1 phase might be involved in actively sustaining the pluripotent state (Calder et al., 2013; Coronado et al., 2013; Singh et al., 2013). However, heterogeneity of PSCs and spatio-temporal patterns of cell cycle dynamics have not yet been investigated.

In this study, I introduced fluorescent ubiquitination-based cell cycle indicator (Fucci) probes (Sakaue-Sawano et al., 2008) into PSCs using lentiviral vectors and measured the length of each cell cycle phase in individual cells by time-lapse imaging. In addition, I compared the length of each cell cycle phase in sequential cell division. I also analyzed the influence of cell density on cell cycle progression.

Materials and Methods

Cell lines

Mouse ESCs (mESCs) (ROSA-mES), rabbit ESCs (rESCs) (rES8-2), rabbit iPSCs (riPSCs) (iPS-S1), naïve-like riPSCs (l-iPS-S) were obtained from Bioresource Engineering Division, BioResource Center, RIKEN. Human ESCs (hESCs) (hES-H1) and normal human skin fibroblasts (NB1RGB) were obtained from CELL BANK, BioResource Center, RIKEN. Human hiPSCs (hiPSCs) (hiPS-PDL24) were generated from NB1RGB by introducing hOCT3/4, hSOX2, hKLF4, and hMYC using lentiviral vectors (Fujioka et al., 2010). Mouse iPSCs (miPSCs) (ROSA-miPS) were generated from mouse embryonic fibroblast (ROSA-MEF) by introducing mOct3/4, mSox2, mKlf4, and m-Myc using lentiviral vectors. All of those cell lines were validated to form teratomas and expressed the endogenous pluripotent markers.

Cell culture

Primed PSCs were plated onto mitomycin-C-treated MEF at a concentration of 6×10^3/cm (rESCs, riPSCs), 2×10^4/cm (hESCs, hiPSCs) on the 0.1% gelatin coated dish. The culture medium of primed PSCs was generated by including 78% DMEM/F12 (Invitrogen), 20% KSR (Invitrogen), 2mM L-Glutamine (Invitrogen), 0.1mM NEAA (Invitrogen), 0.1mM 2-Mercaptoethanol (Sigma), 8ng/ml bFGF (Wako). Passage of hESCs and hESCs was performed by dissociated solution including 0.25% trypsin, 0.1% collagenase type IV, 20% KSR, 1mM CaCl2, PBS(-). Passage of rESCs and rESCs was performed by 0.25% Trypsin-EDTA (Invitrogen). Naïve and naïve-like PSCs were plated onto mitomycin-C-treated MEF at a concentration of 4×10^4/cm on the 0.1% gelatin coated dish. The culture medium of naïve and naïve-like PSCs was generated by including 48% DMEM/F12 (Invitrogen), 48% Neurobasal (Invitrogen), 1% N2 supplement (Invitrogen), 2% B27 supplement (Invitrogen), 10 ng/ml recombinant human LIF (WAKO), 2mM L-Glutamine (Invitrogen), 0.1mM NEAA (Invitrogen), 0.1mM 2-Mercaptoethanol (Sigma), 5 mg/mL BSA (Sigma), 1 μM PD0325901 (WAKO), 3 μM CHIR99021 (WAKO) (and 10 μM Forskolin (WAKO) in case of naïve-like PSCs). Passage of naïve and naïve-like PSCs was performed by 0.25% Trypsin-EDTA (Invitrogen)

Conversion of hiPSCs to naive-like hiPSCs

Naïve-like hiPSCs (nhiPS-2iOF) were generated from hiPS-PDL24 using established methods (Hanna et al., 2010; Honda et al., 2013). hiPSCs were transduced

by a lentiviral vector expressing hOCT3/4-IRES-Venus. About one week after, Venus-positive cells were sorted or picked up, and cultured about one week in primed PSCs medium. After colony formation, culture medium was replaced by naïve medium contained forskolin, and naïve PSCs-like colonies were picked up.

Conversion of miPSCs to mEpiSCs

mEpiSCs (mEpiSC-derived-iPS) were differentiated from ROSA-miPSCs using established methods (Brons et al., 2007; Turco et al., 2012). Briefly, miPSCs were plated onto mitomycin-C-treated MEF at a concentration of 2×10^4/cm on the 15 μg/ml of human fibronectin coated dish. mEpiSCs were cultured on naïve PSCs medium supplemented with 10 ng/ml Activin (R&D systems) and 12ng/ml bFGF (Wako), instead of PD0325901, CHIR99021 and LIF. mEpiSCs were passaged every three days with dissociated solution at least seven times.

Lentiviral vectors

Replication-defective, self-inactivating lentiviral vectors were used (Miyoshi et al., 1998). Fucci cDNA: mCherry-hCdt1(30/120), mCherry-hCdt1(1/100)_CyAAA, mVenus-hGem(1/110), and AmCyan-hGem(1/110) were cloned into the CSII-EF-MCS vector. Reprogramming factor cDNAs: hOct3/4, hSox2, hKlf4, and h-Myc were cloned into the CSII-EF-MCS-IRES-Venus vector. The vector plasmid was co-transfected with the packaging plasmid (pCAG-HIVgp) and the VSV-G into 293T cells. High-titer viral solutions for each cDNA were prepared and used for co-transduction into the cell lines.

Time-lapse imaging and analysis of Cell Cycle

After infection of lentiviral vectors, PSCs were analyzed and sorted using BD LSR II and FACS Aria III (Becton Dickinson). Sorted PSCs were cultured on CELLview 35 mm glass bottom dish (Greiner) coated 0.1% gelatin or 15 μg/ml of human fibronectin. Time-lapse imaging was performed using a computer-assisted fluorescence microscope, LCV110 (Olympus), FV1000d(Olympus), or BZ-9000 (KEYENCE). Image acquisition and analysis were performed using MetaMorph (Universal Imaging, Media, PA), FLUOVIEW Viewer (Olympus), Image J (Schneider et al., 2012), and R software (Jobb et al., 2004).

Results

Cell cycle analysis of PSCs

To analyze cell cycle of naïve PSCs (mESCs/miPSCs) and primed PSCs (mEpiSCs, hESCs/hiPSCs, and rESCs/riPSCs), PSCs were transduced with lentiviral vectors expressing Fucci4 probes under the EF-1 promoter. Fucci4 probes consists of two chimeric proteins: mCherry-hCdt1(1/100)_CyAAA and AmCyan-hGeminine(1/110), which labels G_1 phase nuclei red, S phase nuclei blue, and G_2/M phase nuclei red and blue (Fig. 2-2). PSCs expressed Fucci4 probes at moderate levels were isolated and time-lapse imaging was performed for 48-72 hours.

After processing time-lapse imaging movies (Fig 2-5), I measured the length of each cell cycle phase in individual mouse PSCs. As expected, a prolonged G_1 phase was observed in a significant number of mEpiSCs (Fig 2-6), and the mean length of the G_1 phase of mEpiSCs (3.03±1.45 h) was significantly longer than that of mESCs (2.41±0.79 h) and miPSCs (2.35±0.74 h) (Table 1). On the other hand, there was not much difference in the length of S and G_2/M phases between mESCs/miPSCs and mEpiSCs. In human PSCs (hESCs/hiPSCs) (Fig. 2-7, 8), a significant number of cells with prolonged G_1 phase were also observed (Fig. 2-9). The mean length of the G_1 phase of hESCs (3.50±1.09 h) and hiPSCs (4.31±1.85 h) was longer than that of mEpiSCs (Table 1), but distributions of the G_1 length were similar to mEpiSCs. In rabbit PSCs (rESCs/riPSCs) that can be dissociated into single cells as in naïve PSCs (Fig. 2-10, 11), the mean length of the G_1 phase of rESCs (3.02±0.75 h) and riPSCs (2.93±1.28 h) was similar to that of mEpiSCs (Table 1), but the number of cells with prolonged G_1 phase was decreased as compared to mEpiSCs and hESCs/iPSCs (Fig. 2-12). Again, there was not much difference in the length and distribution of S and G_2/M phases among hESCs/hiPSCs and rESCs/riPSCs. Similar results were obtained with hiPSCs using Fucci2 probes.

Next, I generated naïve-like hiPSCs that can be dissociated into single cells (Fig. 2-14). Fucci4 probes were introduced into naïve-like hiPSCs and riPSCs using lentiviral vectors, and time-lapse imaging was performed (Fig. 2-15, 16). The mean length of the G_1 phase of naïve-like hiPSCs (3.31±1.29 h) and naïve-like riPSCs (3.26±0.81 h) was shorter than corresponding primed iPSCs (Table 1) though cells with prolonged G_1 phase were still observed (Fig. 2-17).

Comparison of the G_1 phase length in sequential cell division

Next, I compared the length of the G_1 phase in sequential cell division of

hiPSCs. No correlation was observed in the length of the G_1 phase in three sequential G_1 phases or in two daughter cells derived from the same mother cell (Fig. 2-18). No correlation was also observed between the G_1 phase and S or G_2/M phases in individual cells (Fig. 2-19). Similar results were obtained with other naïve and primed PSCs (data not shown). These results indicated that the G_1 phase length had no affect on the length of each cell cycle phase in sequential cell division.

Correlation between the cell density and the prolonged G_1 phase

In hiPSCs and mEpiSCs, cells with prolonged G_1 phase were frequently observed in the middle of the colony where the cell density is higher than other locations (Fig. 2-20). Therefore, correlation between the cell density and the length of the G_1 phase was analyzed. The cell density is defined as the number of cells within a circle with 20, 30, or 40 μm diameter from a selected cell in each time-lapse frame (Fig. 2-21, 22). The average cell density was calculated during the G_1 phase or S/G_2/M phases in each time-laps frame (Fig. 2-23a).

The G_1 phase length was likely to increase in proportion to the cell density (Fig. 2-23b). No correlation was observed between the cell density and the length of the S/G_2/M phases. The results suggest that the prolonged G_1 phase is due to contact inhibition.

To compare with differentiated somatic cells, Fucci2 probes (Fig. 2-2) were introduced into HeLa (human epithelial carcinoma cell line) and NMuMG (normal mouse mammary epithelial cell line) using lentiviral vectors, and time-lapse imaging was performed (Fig. 2-24, 25). The G_1 phase length increased in direct proportion to the cell density in HeLa and NMuMG cells as expected (Fig. 2-26a, b). There was a clear difference between hiPSCs and HeLa or NMuMG in terms of the cell density effect on the G_1 phase length. The G_1 phase length of hiPSCs also increased substantially with increasing cell density, but cells with a short G_1 phase also exist at high cell density (Fig. 2-26c). The G_1 phase length of human iPS cells is significantly shorter than that of HeLa and NMuMG cells at high cell density. Because of the technical difficulties, it was not possible to measure the cell density of naïve PSCs with compact and domed colony morphology, but no correlation between the cell density and the G_1 phase length is predicted (Fig. 2-26d).

Discussion

It has been demonstrated that PSCs have unique cell cycle properties characterized by a rapid proliferation with a very short G_1 phase (Savatier et al., 1994; White et al., 2005), suggesting a functional correlation with self-renewal and pluripotency (Calder et al., 2013; Coronado et al., 2013; Singh et al., 2013). However, cell cycle of PSCs has not been analyzed in detail at single cell levels.

In this study, I measured the length of each cell cycle phase in individual PSCs by time-lapse imaging with Fucci probes. The results showed that the mean length of the G_1 phase of primed PSCs was significantly longer than that of naïve PSCs. Heterogeneity was found largely in primed PSCs, in which a significant number of cells with prolonged G_1 phase were observed. In addition, the mean length of the G_1 phase of naïve-like iPSCs was shorter than corresponding primed iPSCs though cells with prolonged G_1 phase were also observed. Intriguingly, there is no correlation in the length of the G_1 phase between mother and daughter cells. Taken together, the results suggest that the prolonged G_1 phase is closely related to the state of PSCs.

In general, proliferation of differentiated somatic cells is responsive to exogenous proliferation signals. Excessive proliferation signals through cell-cell interactions arrest cells in G1 phase or enter cells in quiescent G_0 phase (Fig. 2-27). It has been suggested that contact inhibition is induced by E-cadherin mediated cell-cell contact and intracellular signal transduction pathway (Navarro et al., 1991; Aoki K et al., 2013). In contrast, naïve PSCs (mESCs) are less reliant on exogenous growth factors and are not subject to contact inhibition (Savatier et al., 1994; Schratt et al., 2001; White et al., 2005) (Fig. 2-28). This may be owing to an autocrine loop of PSC growth factor signaling, or a cell autonomous mode of cell division that does not require such signaling cascades. It has been shown that, unlike somatic cells, constitutive Cdk activities in mESCs lead to an inactivation of Rb family member proteins. This results in cell cycle-independent expression of E2F-regulated genes (White et al., 2005). On the other hand, my results showed that the G_1 phase length of some but not all primed PSCs (hiPSCs and mEpiSCs) is affected by the cell density (Fig. 2-29). Therefore, the prolonged G_1 phase cased by contact inhibition may exhibit some differences in cell cycle regulation between naïve and primed PSCs. Indeed, it has been reported that naïve and primed PSCs differ in global gene expression patterns including micro RNAs, X chromosome inactivation pattern, and signaling pathways required for self-renewal (Nichols J et al., 2009).

In conclusion, the results in this study suggest that a short G_1 phase, which is

not affected by the cell density, can be a novel feature of naïve state and might be useful as a marker for evaluation of the state of PSCs in vitro (Fig. 2-30).

Acknowledgements

I would like to thank Professor Hiroyuki Miyoshi and Kazuto Nakada (University of Tsukuba) for supervision of the course for doctoral degree. I wish to thank Dr Atsushi Miyawaki (RIKEN Brain Science Institute), Dr Asako Sakaue-Sawano (RIKEN Brain Science Institute), Dr Naomi Yoshida (RIKEN BioResource Center), Dr Arata Honda (RIKEN BioResource Center), Mrs. Sumie Togayachi (RIKEN BioResource Center), Mrs. Mamiko Kabasawa, Mrs. Kaoru Saijo, Dr Shinichi Noda for assistance and discussion. I wish to thank Dr Yukio Nakamura (RIKEN BioResource Center) for the gift of the human HSCs. I wish to thank Dr Atsuo Ogra, (RIKEN BioResource Center), Dr Michiko Hirose for the gift of the rabbit PSCs. I wish to thank all member of Subteam for Manipulation of Cell Fate (RIKEN BioResource Center), Laboratory for Cell Function and Dynamics, Advanced Technology Development Group (RIKEN Brain Science Institute).

Reference

Abdelalim EM. (2013) Molecular mechanisms controlling the cell cycle in embryonic stem cells. Stem Cell Rev 9, 764-773.

Aoki K, Kumagai Y, Sakurai A, Komatsu N, Fujita Y, Shionyu C, Matsuda M. (2013) Stochastic ERK activation induced by noise and cell-to-cell propagation regulates cell density-dependent proliferation. Molecular Cell 52(4):529-540.

Askew V. (2008) Technology Watch: Fluorescent cycling. Nature Reviews Molecular Cell Biology 9:1038.

Becker KA, Ghule PN, Therrien JA, Lian JB, Stein JL, van Wijnen AJ, Stein GS. (2006). Self-renewal of human embryonic stem cells is supported by a shortened G_1 cell cycle phase. J. Cell. Physiol. 209, 883–893.

Benmaamar R, Pagano M. (2005) Involvement of the SCF complex in the control of ^{Cdh1} degradation in S-phase. Cell Cycle 4(9):1230-1232.

Blomen VA, Boonstra J. (2007). Cell fate determination during G_1 phase progression. Cell Mol Life Sci 64:3084–3104.

Boisset JC, Robin C. (2012) On the origin of hematopoietic stem cells: progress and controversy. Stem Cell Res 8:1-13.

Bouniol C, Nguyen E, Debey P. (1995) Endogenous transcription occurs at the 1-cell stage in the mouse embryo. Exp Cell Res. 218(1):57-62.

Bowie MB, Kent DG, Dykstra B, McKnight KD, McCaffrey L, Hoodless PA, Eaves CJ. (2007) Identification of a new intrinsically timed developmental checkpoint that reprograms key hematopoietic stem cell properties. Proc. Natl. Acad. Sci. USA. 104:5878–5882.

Brons IG, Smithers LE, Trotter MW, Gunn RP, Sun B, Lopes SM, Howlett SK, Clarkson A, Richter LA, Pedersen RA, Vallier L (2007) Derivation of pluripotent epiblast stem cells from mammalian embryos. Nature 448:191–195.

Buecker C, Chen HH, Polo JM, Daheron L, Bu L, Barakat TS, Okwieka P, Porter A, Gribnau J, Hochedlinger K, Geijsen N. (2010). A murine ESC-like state facilitates transgenesis and homologous recombination in human pluripotent stem cells. Cell Stem Cell 6:535-546.

Calder A, Roth-Albin I, Bhatia S, Pilquil C, Lee JH, Bhatia M, Levadoux-Martin M, McNicol J, Russell J, Collins T, Draper JS. (2013). Lengthened G_1 phase indicates differentiation status in human embryonic stem cells. Stem Cells Dev. 22, 279–295.

Cancelas JA, Lee AW, Prabhakar R, Stringer KF, Zheng Y, Williams DA. (2005) Rac GTPases differentially integrate signals regulating hematopoietic stem cell localization. Nature Medicine 11:886–891.

Cheshier SH, Morrison SJ, Liao X, Weissman IL. (1999) In vivo proliferation and cell cycle kinetics of long-term self-renewing hematopoietic stem cells. Proc. Natl. Acad. Sci. USA. 96:3120–3125.

Copley MR1, Beer PA, Eaves CJ. (2012) Hematopoietic stem cell heterogeneity takes center stage. Cell Stem Cell 10:690–697.

Coronado D, Godet M, Bourillot PY, Tapponnier Y, Bernat A, Petit M, Afanassieff M, Markossian S, Malashicheva A, Iacone R, Anastassiadis K, Savatier P. (2013) A short G_1 phase is an intrinsic determinant of naïve embryonic stem cell pluripotency. Stem Cell Research 10(1):118-131.

Curr. Issues Mol. Biol. 3(3): 67-70.

Ema H, Takano H, Sudo K, Nakauchi H. (2000) In vitro self-renewal division of hematopoietic stem cells. J Exp Med 192:1281-1288.

Ema H1, Morita Y, Yamazaki S, Matsubara A, Seita J, Tadokoro Y, Kondo H, Takano H, Nakauchi H. (2006) Adult mouse hematopoietic stem cells: purification and single-cell assays. Nat Protoc 1:2979-2987.

Evans MJ, Kaufman MH. (1981) Establishment in culture of pluripotential cells from

mouse embryos. Nature 292:154–156.

Fagotto F, Rohani N, Touret AS, Li R. (2013) A molecular base for cell sorting at embryonic boundaries: contact inhibition of cadherin adhesion by ephrin/ Eph-dependent contractility. Dev Cell 27:72-87.

Fluckiger AC, Marcy G, Marchand M, Négre D, Cosset FL, Mitalipov S, Wolf D, Savatier P, Dehay C. (2006) Cell cycle features of primate embryonic stem cells. Stem Cells 24, 547–556.

Fujioka T, Shimizu N, Yoshino K, Miyoshi H, Nakamura Y. (2010) Establishment of induced pluripotent stem cells from human neonatal tissues. Hum Cell 23:113-118.

Fujishiro S, Nakano K, Mizukami Y, Azami T, Arai Y, Matsunari H, Ishino R, Nishimura T. (2013) Generation of Naive-Like Porcine-Induced Pluripotent Stem Cells Capable of Contributing to Embryonic and Fetal Development. Stem Cells and Development 22: 473-482.

Gafni O, Weinberger L, Mansour AA, Manor YS, Chomsky E, Ben-Yosef D, Kalma Y, Viukov S, Maza I, Zviran A, Rais Y, Shipony Z, Mukamel Z, Krupalnik V, Zerbib M, Geula S, Caspi I, Schneir D, Shwartz T, Gilad S, Amann-Zalcenstein D, Benjamin S, Amit I, Tanay A, Massarwa R, Novershtern N, Hanna JH. (2013) Derivation of novel human ground state naive pluripotent stem cells. Nature 504:282-286.

Ge WP, Miyawaki A, Gage FH, Jan YN, Jan LY. (2012) Local generation of glia is a major astrocyte source in postnatal cortex. Nature 484:376-380.

Geiger H, de Haan G, Florian MC. (2013) The ageing haematopoietic stem cell compartment. Nat Rev Immunol 13:376-389.

Ghule PN, Medina R, Lengner CJ, Mandeville M, Qiao M, Dominski Z, Lian JB, Stein JL, van Wijnen AJ, Stein GS. (2011) Reprogramming the Pluripotent Cell Cycle: Restoration of an Abbreviated G_1 Phase in Human Induced Pluripotent Stem (iPS) Cells J Cell Physiol 226:1149-1156.

Guo G, Yang J, Nichols J, Hall JS, Eyres I, Mansfield W, Smith A. (2009) Klf4 reverts

developmentally programmed restriction of ground state pluripotency. Development 136(7):1063–1069.

Hanna J, Cheng AW, Saha K, Kim J, Lengner CJ, Soldner F, Cassady JP, Muffat J, Carey BW , Jaenisch R. (2010). Human embryonic stem cells with biological and epigenetic characteristics similar to those of mouse ESCs. Proc Natl Acad Sci USA 107:9222–9227.

Hama H, Kurokawa H, Kawano H, Ando R, Shimogori T, Noda H, Fukami K, Sakaue-Sawano A, Miyawaki A. (2011) Scale: a chemical approach for fluorescence imaging and reconstruction of transparent mouse brain. Nat Neurosci 14:1481-1488.

Honda A, Hirose M, Inoue K, Ogonuki N, Miki H, Shimozawa N, Hatori M, Shimizu N, Murata T, Hirose M, Katayama K, Wakisaka N, Miyoshi H, Yokoyama KK, Sankai T, Ogura A. (2008). Stable embryonic stem cell lines in rabbits: potential small animal models. Reproductive Biomedicine Online 17(5):706-715.

Honda A, Hirose M, Hatori M, Matoba S, Miyoshi H, Inoue K, Ogura A. (2010) Generation of induced pluripotent stem cells in rabbits: potential experimental models for human regenerative medicine. J Biol Chem 285:31362–31369.

Honda A, Hatori M, Hirose M, Honda C, Izu H, Inoue K, Hirasawa R, Matoba S, Togayachi S, Miyoshi H, Ogura A. (2013) Naive-like Conversion Overcomes the Limited Differentiation Capacity of Induced Pluripotent Stem Cells. The Journal of Biological Chemistry 288(36):26157-26166.

Jobb G, von Haeseler A, Strimmer K. (2004) R: TREEFINDER: a powerful graphical analysis environment for molecular phylogenetics. BMC Evolutionary Biology 28:4-18.

Juuri E, Saito K, Ahtiainen L, Seidel K, Tummers M, Hochedlinger K, Klein OD, Thesleff I, Michon F. (2012) Sox2+ stem cells contribute to all epithelial lineages of the tooth via Sfrp5+ progenitors. Dev Cell 23:317-328.

Kiel MJ, Yilmaz OH, Iwashita T, Yilmaz OH, Terhorst C, Morrison SJ. (2005) SLAM family receptors distinguish hematopoietic stem and progenitor cells and reveal endothelial niches for stem cells. Cell 121:1109-1121.

Kobayashi T, Kageyama R. (2011) Hes1 oscillations contribute to heterogeneous differentiation responses in embryonic stem cells. Genes 2(1):219-228.

Köhler A, Schmithorst V, Filippi MD, Ryan MA, Daria D, Gunzer M, Geiger H. (2009) Altered cellular dynamics and endosteal location of aged early hematopoietic progenitor cells revealed by time-lapse intravital imaging in long bones. Blood 114:290-298.

Kondo M, Wagers AJ, Manz MG, Prohaska SS, Scherer DC, Beilhack GF, Shizuru JA, Weissman IL. (2003) Biology of hematopoietic stem cells and progenitors: Implications for clinical application. Annu Rev Immunol 21:759–806.

Lewis Wolpert. (2011)　Principles of Development Oxford University Press

Lo Celso C, Fleming HE, Wu JW, Zhao CX, Miake-Lye S, Fujisaki J, Côté D, Rowe DW, Lin CP, Scadden DT. (2009) Live-animal tracking of individual haematopoietic stem/progenitor cells in their niche. Nature 457:92-96.

Maxmen A. (2011) Single-cell analysis: Imaging is everything. Nature480,139-141.

Mayle A, Luo M, Jeong M, Goodell MA. (2013) Flow cytometry analysis of murine hematopoietic stem cells. Cytometry A 83:27-37.

Mechali M, Lutzmann M. (2008) The cell cycle: now live and in color. Cell 132:341–343.

Miyoshi H, Blömer U, Takahashi M, Gage FH, Verma IM. (1998). Development of a self-inactivating lentivirus vector. J Virol 72:8150-8157.

Montrone C, Kokkaliaris KD, Loeffler D, Lechner M, Kastenmüller G, Schroeder T, Ruepp A. (2013) HSC-explorer: a curated database for hematopoietic stem cells. PLoS One 8(7):

Morita Y, Ema H, Nakauchi H. (2010) Heterogeneity and hierarchy within the most primitive hematopoietic stem cell compartment. J Exp Med 207:1173-1182.

Morrison SJ, Scadden DT. (2014) The bone marrow niche for haematopoietic stem cells.

Nature 505:327-334.

Navarro P, Gómez M, Pizarro A, Gamallo C, Quintanilla M, Cano A (1991) A role for the E-cadherin cell-cell adhesion molecule during tumor progression of mouse epidermal carcinogenesis. J. Cell Biol. 115:517–533.

Nichols J, Smith A (2009) Naive and primed pluripotent states. Cell Stem Cell 487–492.

Noda S, Horiguchi K, Ichikawa H, Miyoshi H. (2008) Repopulating activity of ex vivo-expanded murine hematopoietic stem cells resides in the CD48-c-Kit+Sca-1+lineage marker- cell population. Stem Cells 26:646-655.

Nunez R. (2001) DNA Measurement and Cell Cycle Analysis by Flow Cytometry.

Nygren JM, Bryder D, Jacobsen SE. (2006) Prolonged cell cycle transit is a defining and developmentally conserved hemopoietic stem cell property. J. Immunol. 177:201–208.

Oki T, Nishimura K, Kitaura J, Togami K, Maehara A, Izawa K, Sakaue-Sawano A, Niida A, Miyano S, Aburatani H, Kiyonari H, Miyawaki A, Kitamura T. (2014) A novel cell-cycle-indicator, mVenus-p27K-, identifies quiescent cells and visualizes G0-G1 transition. Sci. Rep. 4:4012.

Olariu V. (2013) Stem cell dynamics: naïve pluripotency and reprogramming. OA Biology 01:1(1):4.

Osawa M, Hanada K, Hamada H, Nakauchi H. (1996) Long-term lymphohematopoietic reconstitution by a single CD34-low/negative hematopoietic stem cell. Science 273 (1996) 242-245.

Pfeuty B1, David-Pfeuty T, Kaneko K. (2008) Underlying principles of cell fate determination during G_1 phase of the mammalian cell cycle. Cell Cycle 7(20):3246-3257.

Pietras EM, Warr MR, Passegué E. (2011) Cell cycle regulation in hematopoietic stem cells. J Cell Biol. 195(5):709-720.

Ramakrishna V, Janardhan PB Sudarsanareddy L. (2011) Stem Cells and egenerative

Medicine –A Review. Annual Review & Research in Biology 1(4): 79-110.

Ruiz S, Panopoulos AD, Herrerías A, Bissig KD, Lutz M, Berggren WT, Verma IM, Izpisua Belmonte JC. (2011). A high proliferation rate is required for cell reprogramming and maintenance of human embryonic stem cell identity. Curr Biol 21:45–52.

Sakaue-Sawano A, Kurokawa H, Morimura T, Hanyu A, Hama H, Osawa H, Kashiwagi S, Fukami K, Miyata T, Miyoshi H, Imamura T, Ogawa M, Masai H, Miyawaki A. (2008) Visualizing spatiotemporal dynamics of multicellular cell-cycle progression. Cell 132:487–498.

Sakaue-Sawano A, Hoshida T, Yo M, Takahashi R, Ohtawa K, Arai T, Takahashi E, Noda S, Miyoshi H, Miyawaki A. (2013) Visualizing developmentally programmed endoreplication in mammals using ubiquitin oscillators. Development 140(22):4624-4632.

Savatier P, Huang S, Szekely L, Wiman KG, Samarut J. (1994) Contrasting patterns of retinoblastoma protein expression in mouse embryonic stem cells and embryonic fibroblasts. Oncogene 9(3):809-818.

Savatier P, Lapillonne H, van Grunsven LA, Rudkin BB, Samarut J. (1996) Withdrawal of differentiation inhibitory activity/leukemia inhibitory factor up-regulates D-type cyclins and cyclin-dependent kinase inhibitors in mouse embryonic stem cells. Oncogene 12(2):309-22.

Schneider CA, Rasband WS, Eliceiri KW. (2012) NIH Image to ImageJ: 25 years of image analysis". Nature Methods 9: 671-675.

Schratt G, Weinhold B, Lundberg AS, Schuck S, Berger J, Schwarz H, Weinberg RA, Rüther U, Nordheim A. (2001) Serum response factor is required for immediate-early gene activation yet is dispensable for proliferation of embryonic stem cells. Mol Cell Biol. 21(8):2933-2943.

Shizuru JA, Negrin RS, Weissman IL. (2005) Hematopoietic stem and progenitor cells: linical and preclinical regeneration of the hematolymphoidsystem. Annu Rev Med 6:509

–538.

Silva J, Nichols J, Theunissen TW, Guo G, van Oosten AL, Barrandon O, Wray J, Yamanaka S, Chambers I, Smith A. (2009) Nanog is the gateway to the pluripotent ground state. Cell 138(4):722–737.

Singh AM, Chappell J, Trost R, Lin L, Wang T, Tang J, Matlock BK, Weller KP, Wu H, Zhao S, Jin P, Dalton S. (2013) Cell-Cycle control of developmentally regulated transcription factors accounts for heterogeneity in human pluripotent cells. Stem Cell Reports 1(6):532-544.

Smith AG, Heath JK, Donaldson DD, Wong GG, Moreau J, Stahl M, Rogers D. (1988) Inhibition of pluripotential embryonic stem cell differentiation by purified polypeptides. Nature 336(6200):688–690.

Stead E, White J, Faast R, Conn S, Goldstone S, Rathjen J, Dhingra U, Rathjen P, Walker D, Dalton S. (2002) Pluripotent cell division cycles are driven by ectopic Cdk2, cyclin A/E and E2F activities. Oncogene 21(54):8320-8333.

Suvorova II, Katolikova NV, Pospelov VA. (2012) New Insights into Cell Cycle Regulation and DNA Damage Response in Embryonic Stem Cells. International Review of Cell and Molecular Biology 299:161-198.

Symonds CE, Galderisi U, Giordano A. (2009) Aging of the inceptive cellular population: the relationship between stem cells and aging. Aging 1(4):372-381.

Takahashi K, Yamanaka S. (2006) Induction of pluripotent stem cells from mouse embryonic and adult fibroblast cultures by defined factors. Cell 126:663–676.

Takahashi K, Tanabe K, Ohnuki M, Narita M, Ichisaka T, Tomoda K ,Yamanaka S. (2007). Induction of pluripotent stem cells from adult human fibroblasts by defined factors. Cell 131:861–872.

Takano H1, Ema H, Sudo K, Nakauchi H. (2004) Asymmetric division and lineage commitment at the level of hematopoietic stem cells: inference from differentiation in daughter cell and granddaughter cell pairs. J Exp Med 199:295-302.

Takashima Y, Guo G, Loos R, Nichols J, Ficz G, Krueger F, Oxley D, Santos F, Clarke J, Mansfield W, Reik W, Bertone P, Smith A. (2014) Resetting transcription factor control circuitry toward ground-state pluripotency in human. Cell 158:1254-1269.

Tesar PJ, Chenoweth JG, Brook FA, Davies TJ, Evans EP, Mack DL, Gardner RL, McKay RD. (2007) New cell lines from mouse epiblast share defining features with human embryonic stem cells. Nature 448:196–199.

Theunissen TW, Powell BE, Wang H, Mitalipova M, Faddah DA, Reddy J, Fan ZP, Maetzel D, Ganz K, Shi L, Lungjangwa T, Imsoonthornruksa S, Stelzer Y, Rangarajan S, D'Alessio A, Zhang J, Gao Q, Dawlaty MM, Young RA, Gray NS, Jaenisch R. (2014) Systematic identification of defined conditions for induction and maintenance of naïve human pluripotency. Cell Stem Cell 15:471-487.

Thomson JA, J Itskovitz-Eldor, Shapiro SS, Waknitz MA, Swiergiel JJ, Marshall VS, Jones JM. (1998) Embryonic stem cell lines derived from human blastocysts. Science 282:1145–1147.

Turco MY, Furia L, Dietze A, Fernandez Diaz L, Ronzoni S, Sciullo A, Simeone A, Constam D, Faretta M, Lanfrancone L. (2012) Cellular Heterogeneity During Embryonic Stem Cell Differentiation to Epiblast Stem Cells is Revealed by the ShcD/RaLP Adaptor Protein. Stem Cells 30(11):2423-2436.

Wei W1, Ayad NG, Wan Y, Zhang GJ, Kirschner MW, Kaelin WG Jr. (2004) Degradation of the SCF component ^{Skp2} in cell-cycle phase G_1 by the anaphase-promoting complex. Nature 428:194–198.

White J, Dalton S. (2005) Cell cycle control of embryonic stem cells. Stem Cell Reviews 1(2):131-138.

Whitfield ML, George LK, Grant GD, Perou CM. (2006) Common markers of proliferation. Nature Reviews Cancer 6:99-106.

Xie Y, Yin T, Wiegraebe W, He XC, Miller D, Stark D, Perko K, Alexander R, Schwartz J, Grindley JC, Park J, Haug JS, Wunderlich JP, Li H, Zhang S, Johnson T, Feldman RA,

Li L. (2009) Detection of functional haematopoietic stem cell niche using real-time imaging. Nature 457:97-101.

Yamanaka S. (2012) Induced pluripotent stem cells: past, present, and future. Cell Stem Cell. 10(6):678-684.

Ying QL, Nichols J, Chambers I, Smith A. (2003) BMP induction of Id proteins suppresses differentiation and sustains embryonic stem cell self-renewal in collaboration with STAT3. Cell 115(3):281–292.

Ying QL, Wray J, Nichols J, Batlle-Morera L, Doble B, Woodgett J, Cohen P, Smith A. (2008) The ground state of embryonic stem cell self-renewal. Nature 453 (7194):519–523.

Figures

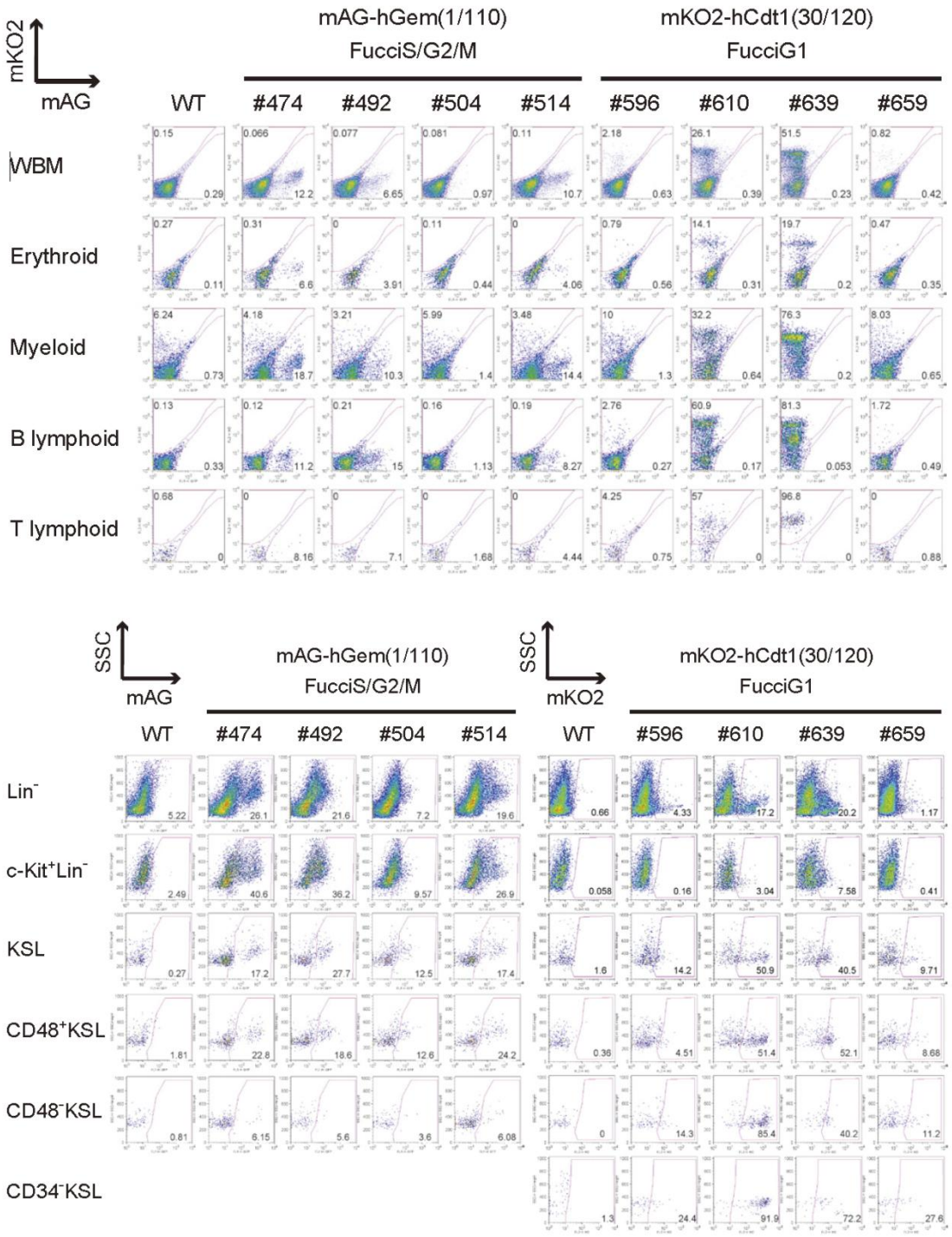
mKO2
mAG
mAG-hGem(1/110)
FucciS/G2/M
mKO2-hCdt1(30/120)
FucciG1
WT
#474
#492
#504
#514
#596
#610
#639
#659
WBM
Erythroid
Myeloid
B lymphoid
T lymphoid
SSC
mAG
mKO2
Lin⁻
c-Kit⁺Lin⁻
KSL
CD48⁺KSL
CD48⁻KSL
CD34⁻KSL

Figure 1-1. FACS analysis of transgene expression in hematopoietic cells of FucciS/G_2/M and FucciG_1 transgenic mice. BM cells were isolated from FucciS/G_2/M transgenic mouse lines (#474, #492, #504, and #514) and FucciG_1 lines (#596, #610, #639, and #659). The cells were stained with cell surface marker antibodies, and FucciS/G_2/M(mAG) or FucciG_1(mKO2) transgene expression was analyzed by flow cytometry. Shown are representative FACS profiles of (A) whole BM, erythroid (Ter119$^+$), myeloid (Gr-1$^+$ or Mac-1$^+$), B-lymphoid (B220$^+$), T-lymphoid (CD4$^+$ or CD8$^+$), (B) Lin$^-$, c-Kit$^+$Lin$^-$, KSL, CD48$^+$KSL, CD48$^-$KSL, and CD34$^-$KSL cells

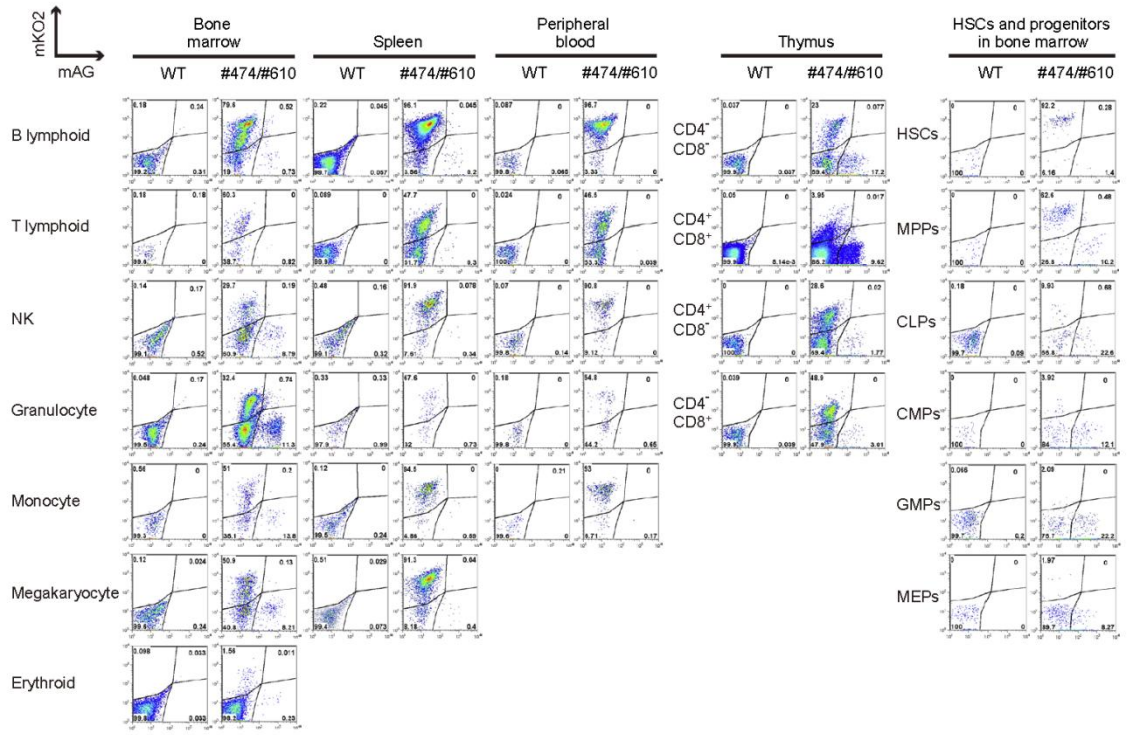

Figure 1-2. FACS analysis of transgene expression in hematopoietic cells of Fucci transgenic mouse line #474/#610. Hematopoietic cells were isolated from BM, spleen, PB, and thymus of Fucci transgenic mouse line #474/#610 and stained with cell surface marker antibodies. Fucci$S/G_2/M$(mAG) and FucciG_1(mKO2) transgene expression was analyzed by flow cytometry. Representative FACS profiles of hematopoietic subpopulations are shown. Gating for hematopoietic subpopulations are shown in Figure 1-4.

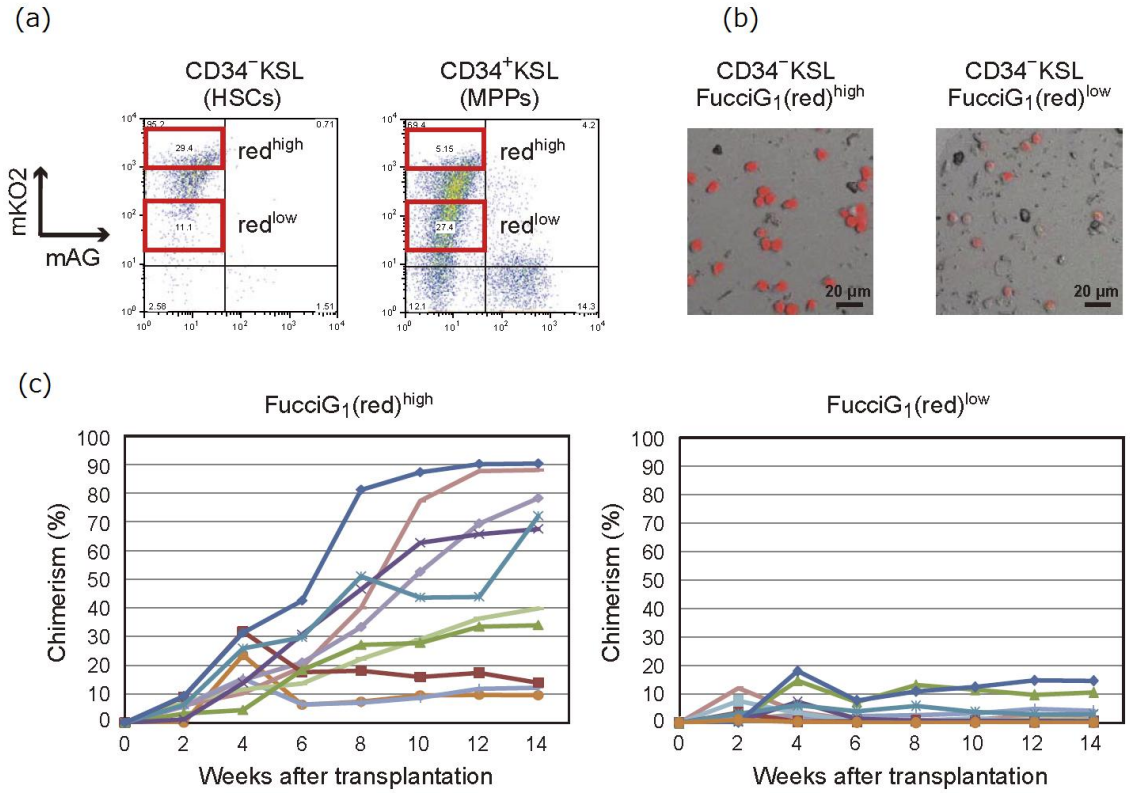

Figure 1-3. FucciG$_1$ fluorescence intensity and repopulating activity of HSCs from Fucci transgenic mouse line #474/#610. (A) FACS profiles of HSC (CD34$^-$KSL) and MPP (CD34$^+$KSL) populations of BM cells from Fucci transgenic mice (#474/#610). FucciG$_1$(red)^{high} and FucciG$_1$(red)^{low} populations are indicated. (B) Representative fluorescence and DIC images of FACS-sorted FucciG$_1$(red)^{high} and FucciG$_1$(red)^{low} CD34$^-$KSL cells. (C) Twenty FACS-sorted FucciG$_1$(red)^{high} or FucciG$_1$(red)^{low} CD34$^-$KSL cells were subjected to a competitive repopulation assay. At the indicated time points after transplantation, PB cells of the recipient mice were analyzed by flow cytometry, and donor chimerism was determined. Data from two independent transplantation experiments are shown (n = 5 or 6 mice per experiment).

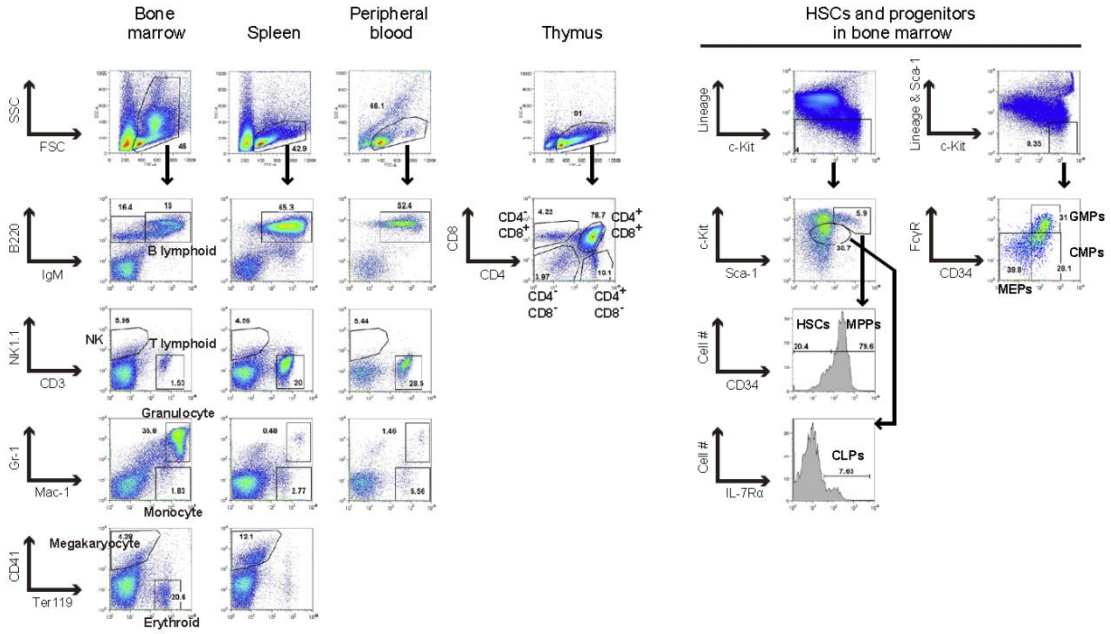

Figure 1-4. Gating for FACS analysis of transgene expression in hematopoietic subpopulations. Hematopoietic cells were isolated from BM, spleen, PB, and thymus of Fucci transgenic mouse line #474/#610 and stained with cell surface marker antibodies as described in Materials and Methods. Shown are representative gating for hematopoietic subpopulations: B-lymphoid cells ($B220^{+}IgM^{+}$), T-lymphoid cells ($CD3^{+}$, $CD4^{-}CD8^{-}$, $CD4^{+}CD8^{-}$, $CD4^{-}CD8^{+}$, and $CD4^{+}CD8^{+}$), NK cells ($NK1.1^{+}$), granulocyte ($Gr\text{-}1^{+}Mac\text{-}1^{+}$), monocyte ($Gr\text{-}1^{-}Mac\text{-}1^{+}$), megakaryocyte ($CD41^{+}$), erythroid cells ($Ter119^{+}$), HSCs ($CD34^{-/low}c\text{-}Kit^{+}Sca\text{-}1^{+}Lin^{-}$), MPPs ($CD34^{+}c\text{-}Kit^{+}Sca\text{-}1^{+}Lin^{-}$), CLPs ($c\text{-}Kit^{mid}Sca\text{-}1^{mid}Lin^{-}IL\text{-}7R\square^{+}$), CMPs ($CD34^{+}c\text{-}Kit^{+}Sca\text{-}1^{-}Lin^{-}Fc\square R^{-}$), GMPs ($CD34^{+}c\text{-}Kit^{+}Sca\text{-}1^{-}Lin^{-}Fc\square R^{+}$), and MEPs ($CD34^{-}c\text{-}Kit^{+}Sca\text{-}1^{-}Lin^{-}Fc\square R^{-}$).

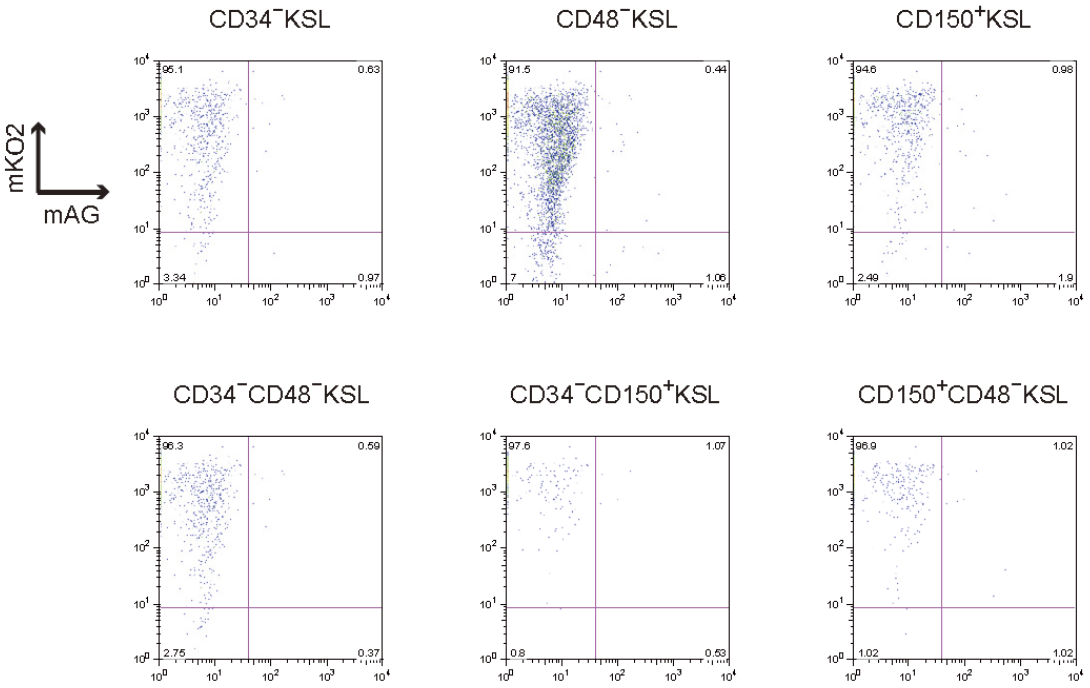

Figure 1-5. FucciG$_1$ fluorescence intensity of HSC populations in Fucci transgenic mouse line #474/#610. BM cells of Fucci transgenic mouse line #474/#610 were stained with the following antibodies: biotinylated anti-lineage markers, PE-Cy5.5-conjugated anti-Sca-1, APC-eFluor780-conjugated anti-c-Kit, eFluor660-conjugated anti-CD34, eFluor450-conjugated anti-CD48, and PE-Cy7-conjugated CD150 (all antibodies purchased from eBioscience). The biotinylated antibodies were developed with V500-conjugated streptavidin (BD Biosciences). The stained cells were analyzed with a FACSAriaIII equipped with four lasers (405, 488, 561, and 633 nm). Representative FACS profiles of HSC populations are shown.

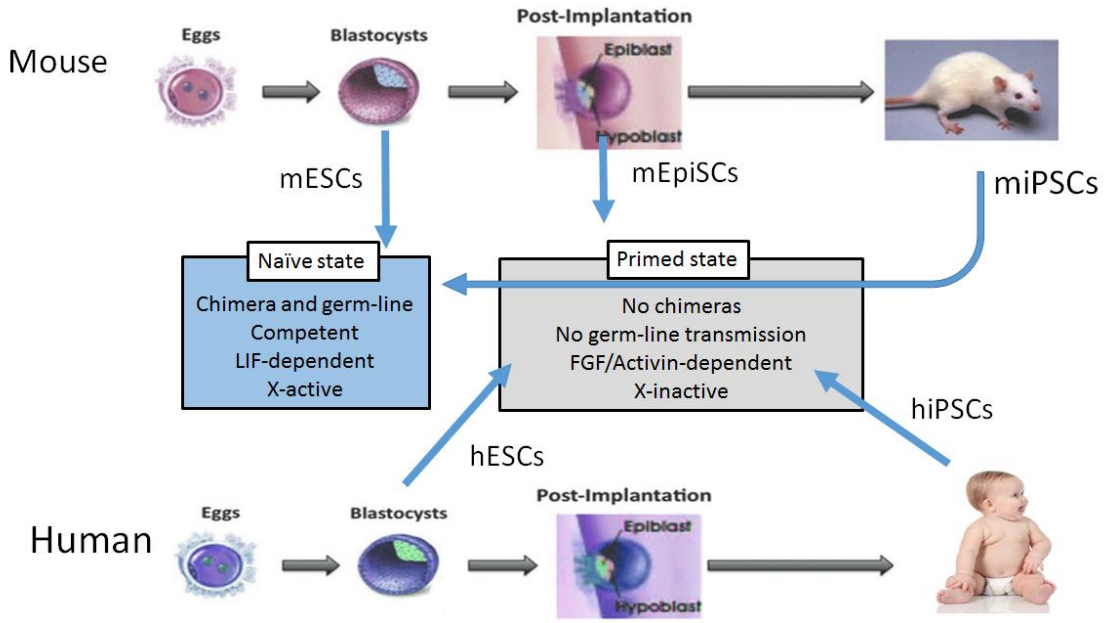

Modified Fujishiro S et al. (2013)

Figure 2-1. Naïve and primed PSCs. In mice, mESCs are derived from the inner cell mass of pre-implantation blastocysts and readily contribute to chimera formation after blastocyst injection (naive state). mEpiSCs are derived from the post-implantation epiblasts. mEpiSCs are also pluripotent stem cells, but they rarely contribute to chimera formation (primed state). Unlike mouse PSCs, ESCs/iPSCs derived from other species, including humans, rabbits, pigs, and primates, are classified as the primed state.

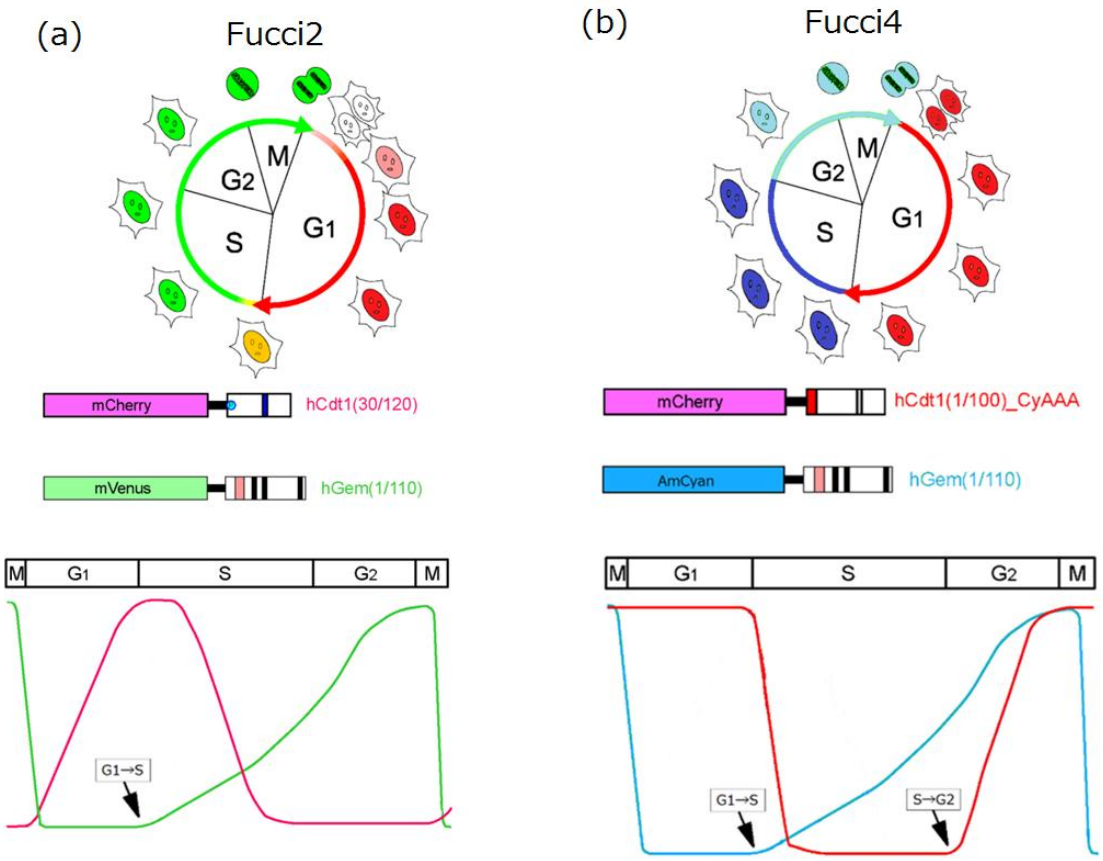

Figure 2-2. Fucci2 and Fucci4. (a) Fucci2 probes consists of mCherry-hCdt1(1/100) and mVenus-hGeminine(1/110). The combinations of fluorescence color and cell cycle phases are G_1-red, S/G_2/M-green, and G_1/S-red and green. (b) Fucci4 consists of mCherry-hCdt1(1/100)_CyAAA and AmCyan-hGeminine (1/110). The combinations of fluorescence color and cell cycle phases are G_1-red, S-blue, and G_2/M-red and blue.

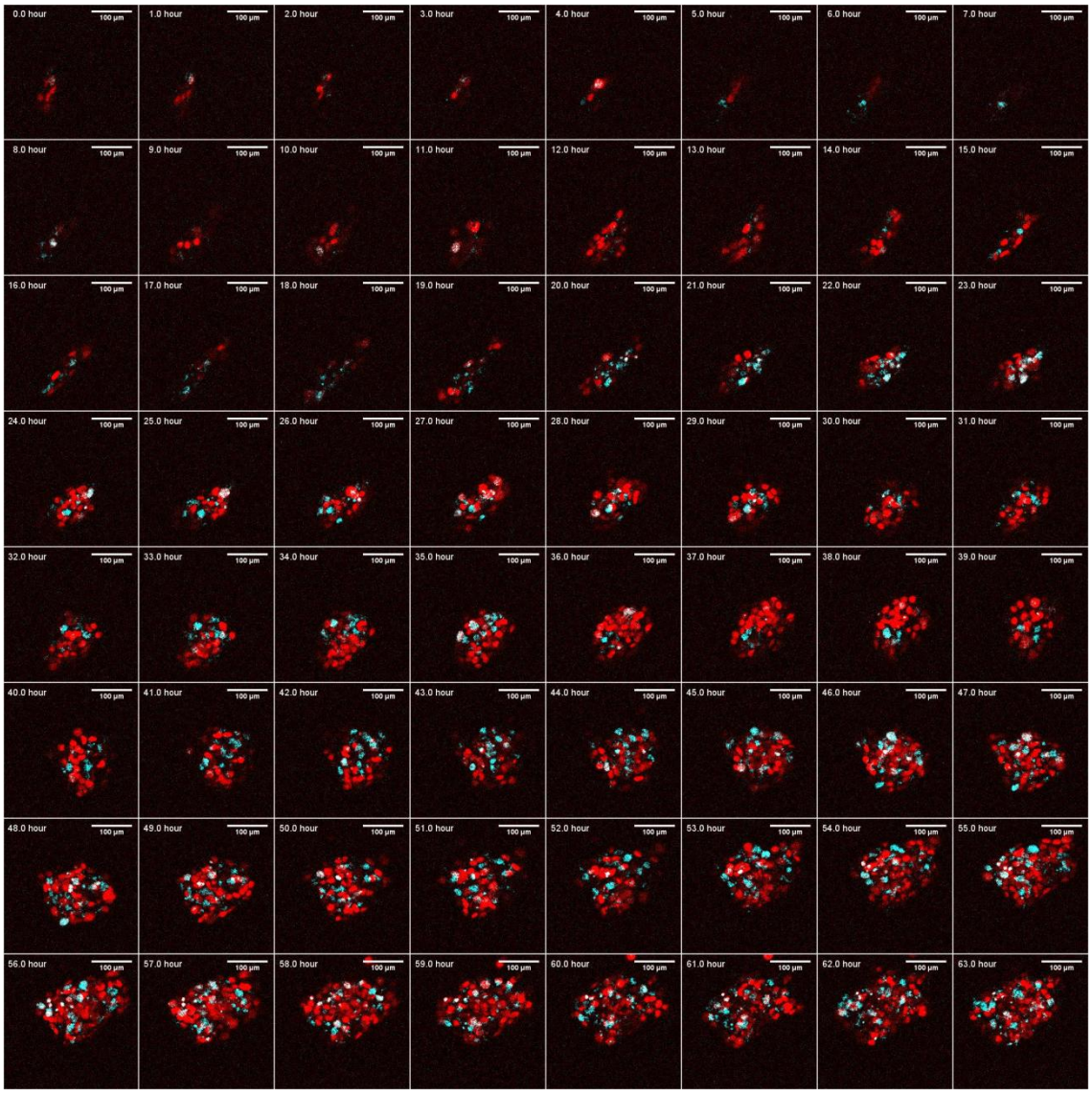

Figure 2-3. Time-lapse imaging of mESCs using Fucci4 probes. Time-lapse imaging of mESCs was performed with FV1000-D confocal microscope for 63 hours. Since Fucci4 probes were used in this imaging, the combinations of fluorescence color and each cell cycle phase are G_1-red, S-blue, and G_2/M-red and blue (the color is processed to white).

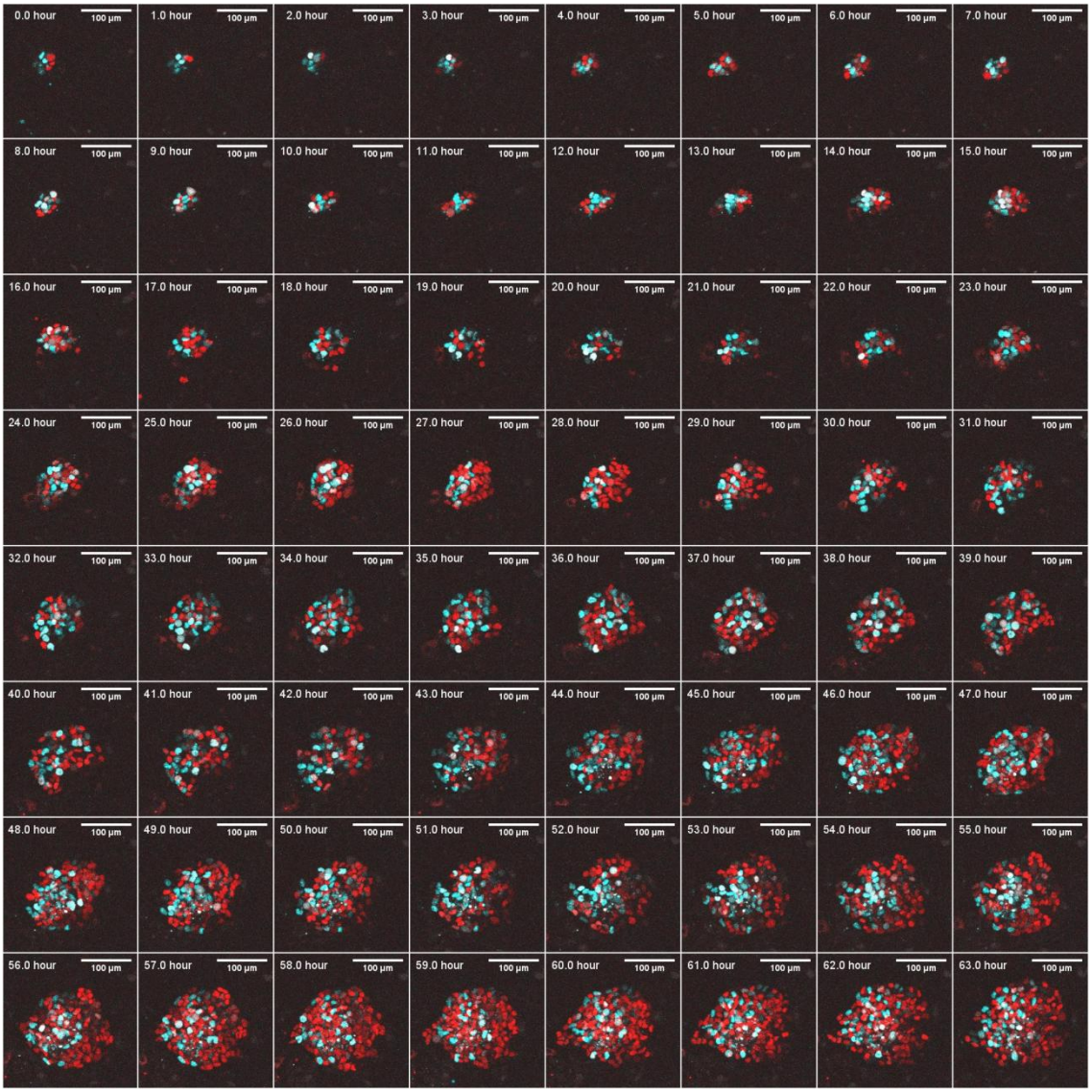

Figure 2-4. Time-lapse imaging of miPSCs using Fucci4 probes. Time-lapse imaging of mESCs was performed with FV1000-D confocal microscope for 63 hours. Since Fucci4 probes were used in this imaging, the combinations of fluorescence color and each cell cycle phase are G_1-red, S-blue, and G_2/M-red and blue (the color is processed to white).

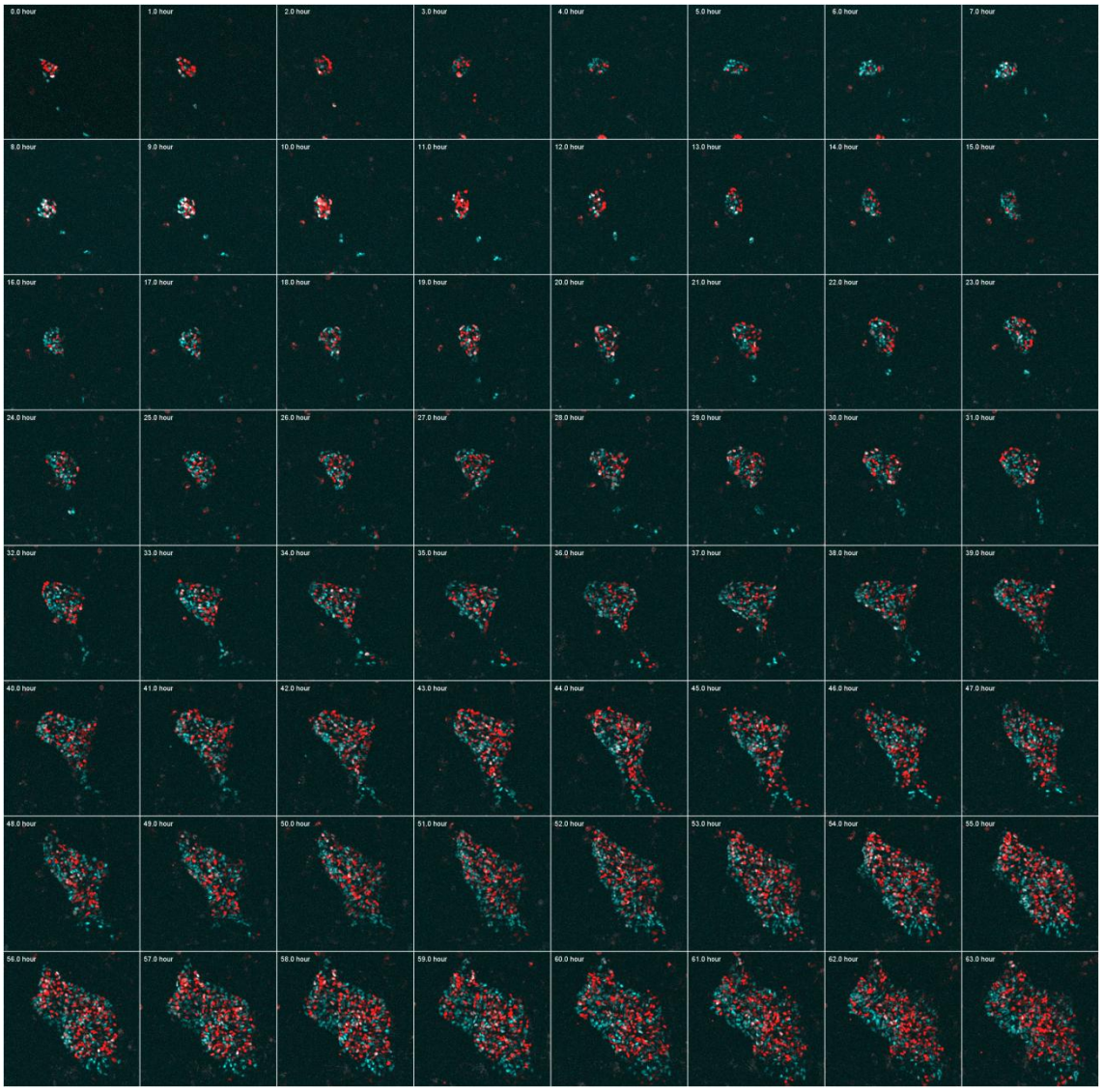

Figure 2-5. Time-lapse imaging of mEpiSCs using Fucci4 probes. Time-lapse imaging of mESCs was performed with FV1000-D confocal microscope for 63 hours. Since Fucci4 probes were used in this imaging, the combinations of fluorescence color and each cell cycle phase are G_1-red, S-blue, and G_2/M-red and blue (the color is processed to white).

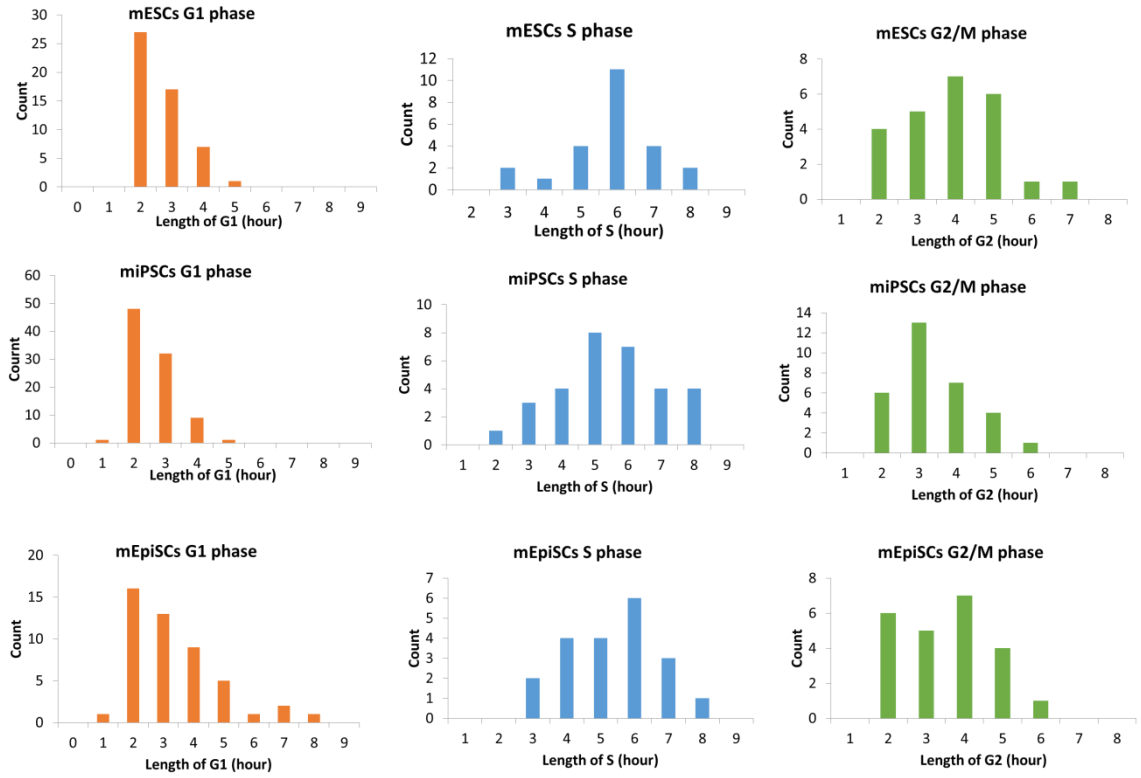

Figure 2-6. The length of each cell cycle phase in individual mouse PSCs. Each line of three graphs is showing distribution of length of G_1, S, and G_2/M phases. Most of mESCs and miPSCs have a very short G_1 phase within 5 hours. On the other hands, a significant number of mEpiSCs have a prolonged G_1 phase more than 5 hours.

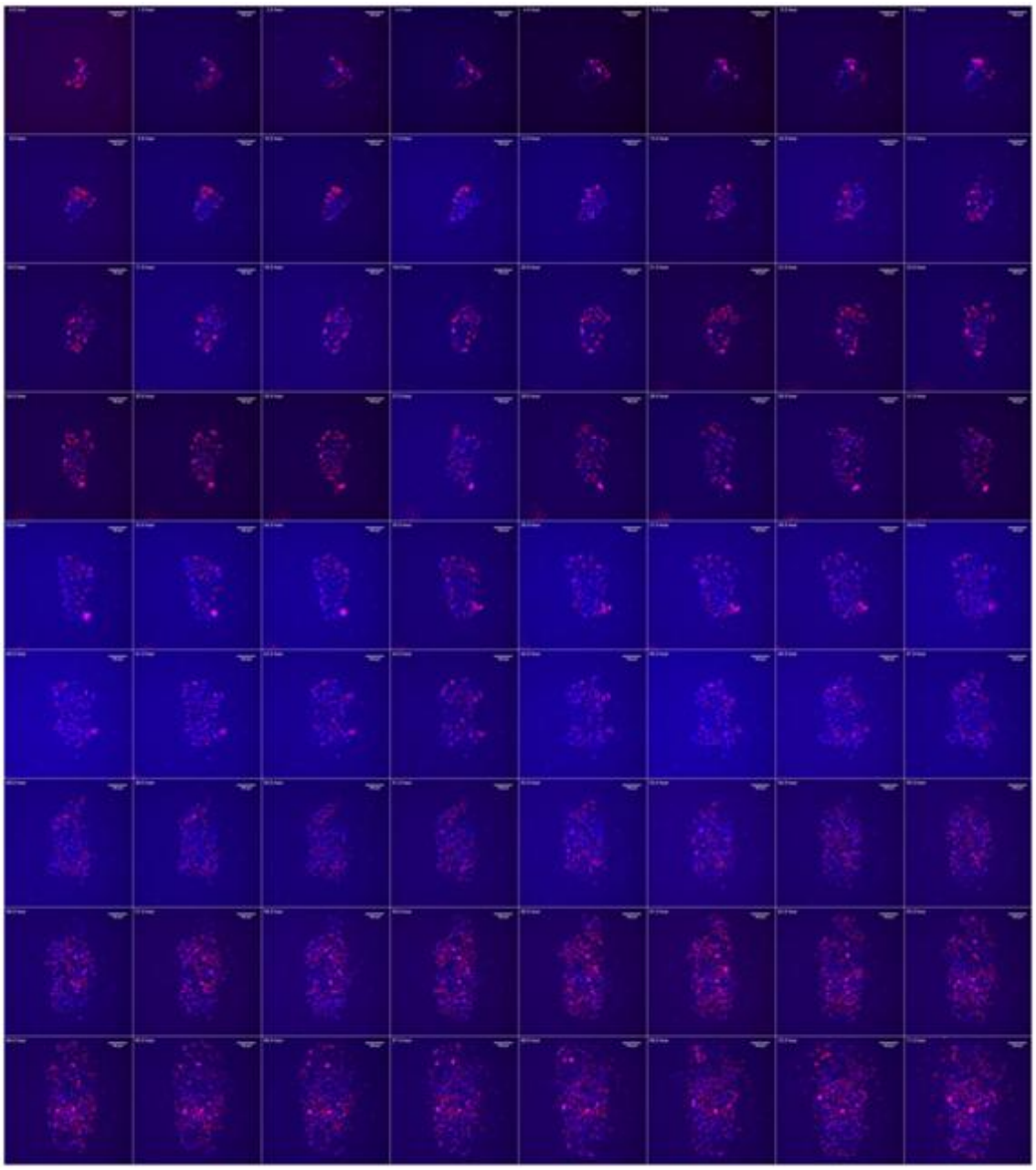

Figure 2-7. Time-lapse imaging of hESCs using Fucci4 probes. Time-lapse imaging was performed with BZ-9000 for 71 hours. Since Fucci4 was used in this imaging, the combinations of fluorescence color and phases of cell cycle are G_1-red, S-blue, G_2/M -red and blue (the color of G_2/M is processed to violet).

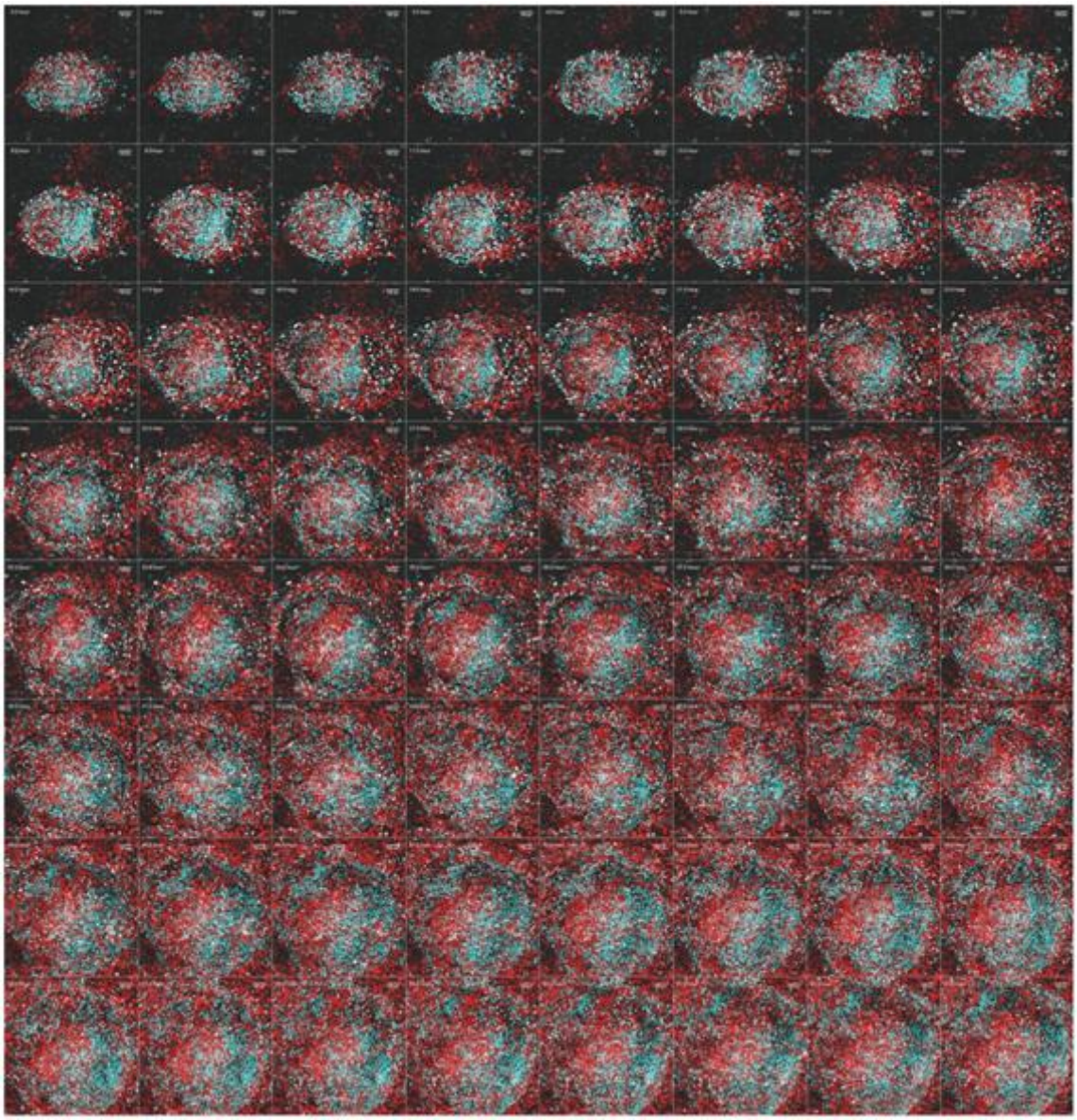

Figure 2-8. Time-lapse imaging of hiPSCs using Fucci4 probes. Time-lapse imaging was performed by FV1000-D for 63 hours. Since Fucci4 was used in this imaging, the combinations of fluorescence color and phases of cell cycle are G_1-red, S-blue, G_2/M-red and blue (the color of G_2/M is processed to white).

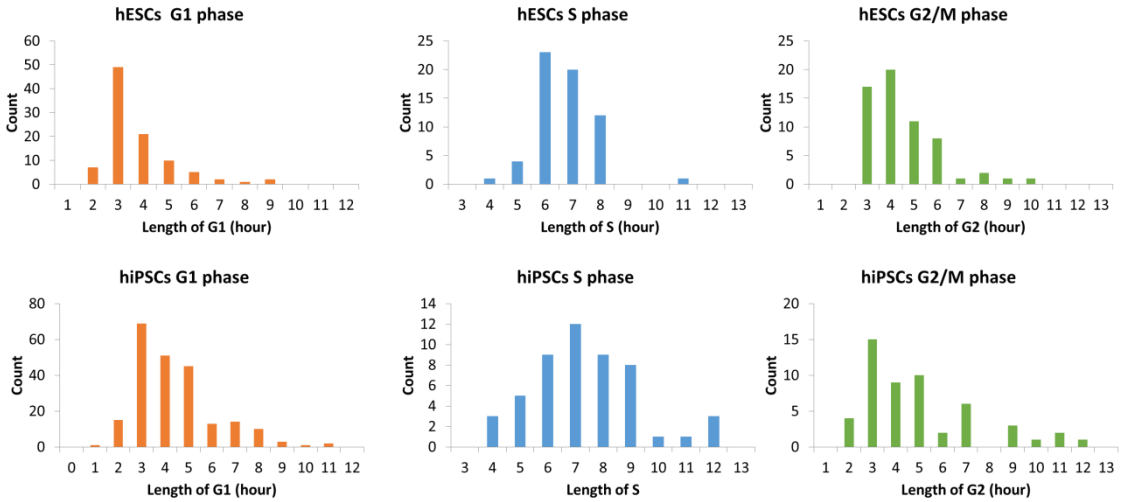

Figure 2-9. The length of each cell cycle phase in individual human PSCs. Each line of three graphs is showing distribution of length of G_1, S, and G_2/M phase. The length of the G_1 length of most hESCs and hiPSCs is 3-4 hours, but distributions of the G_1 length were similar to mEpiSCs and a significant number of cells have a prolonged G_1 phase more than 5 hours.

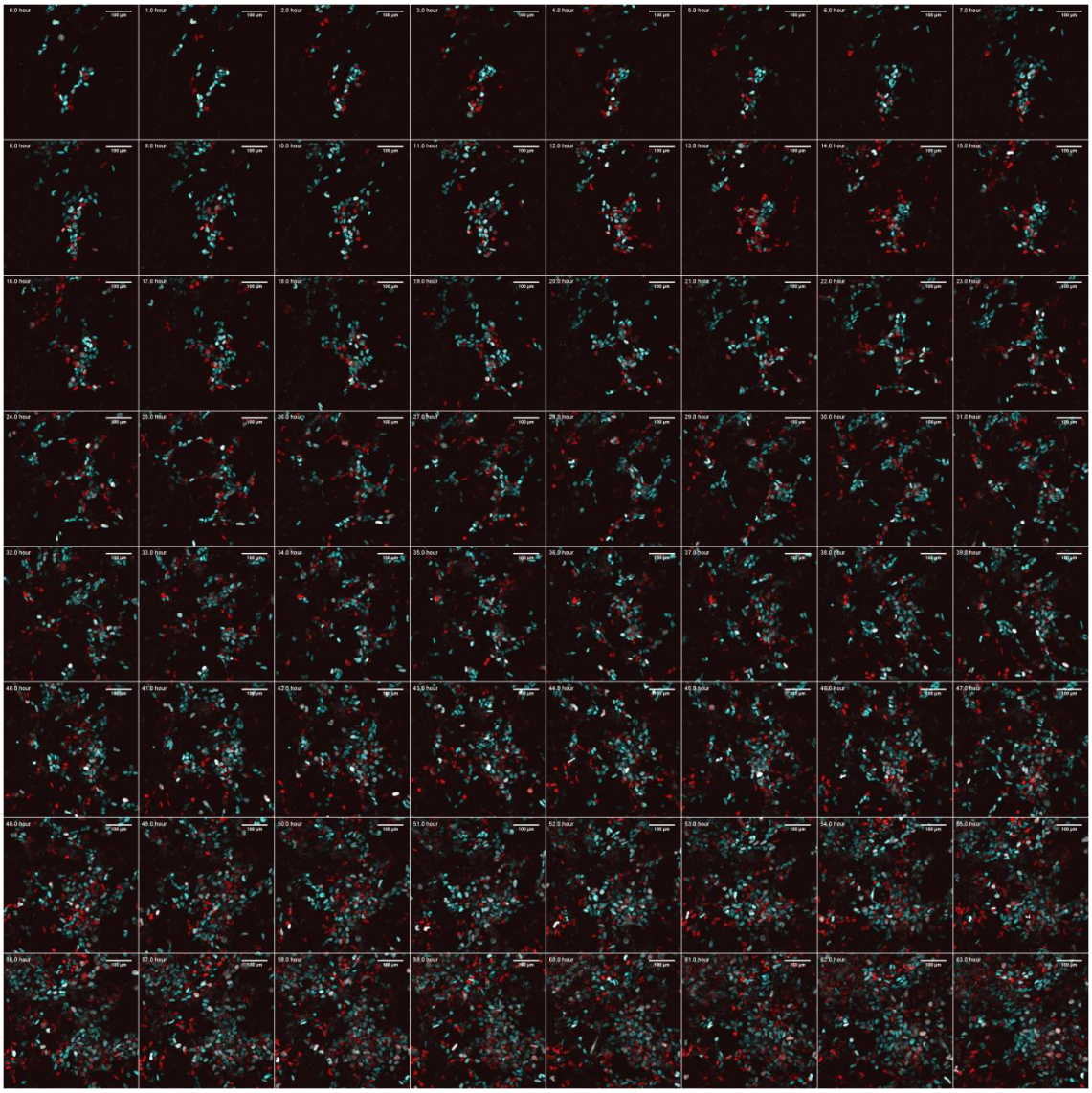

Figure 2-10. Time-lapse imaging of rESCs using Fucci4 probes. Time-lapse imaging was performed by FV1000-D for 63 hours. Since Fucci4 was used in this imaging, the combinations of fluorescence color and phases of cell cycle are G_1-red, S-blue, G_2/M-red and blue (the color of G_2/M is processed to white).

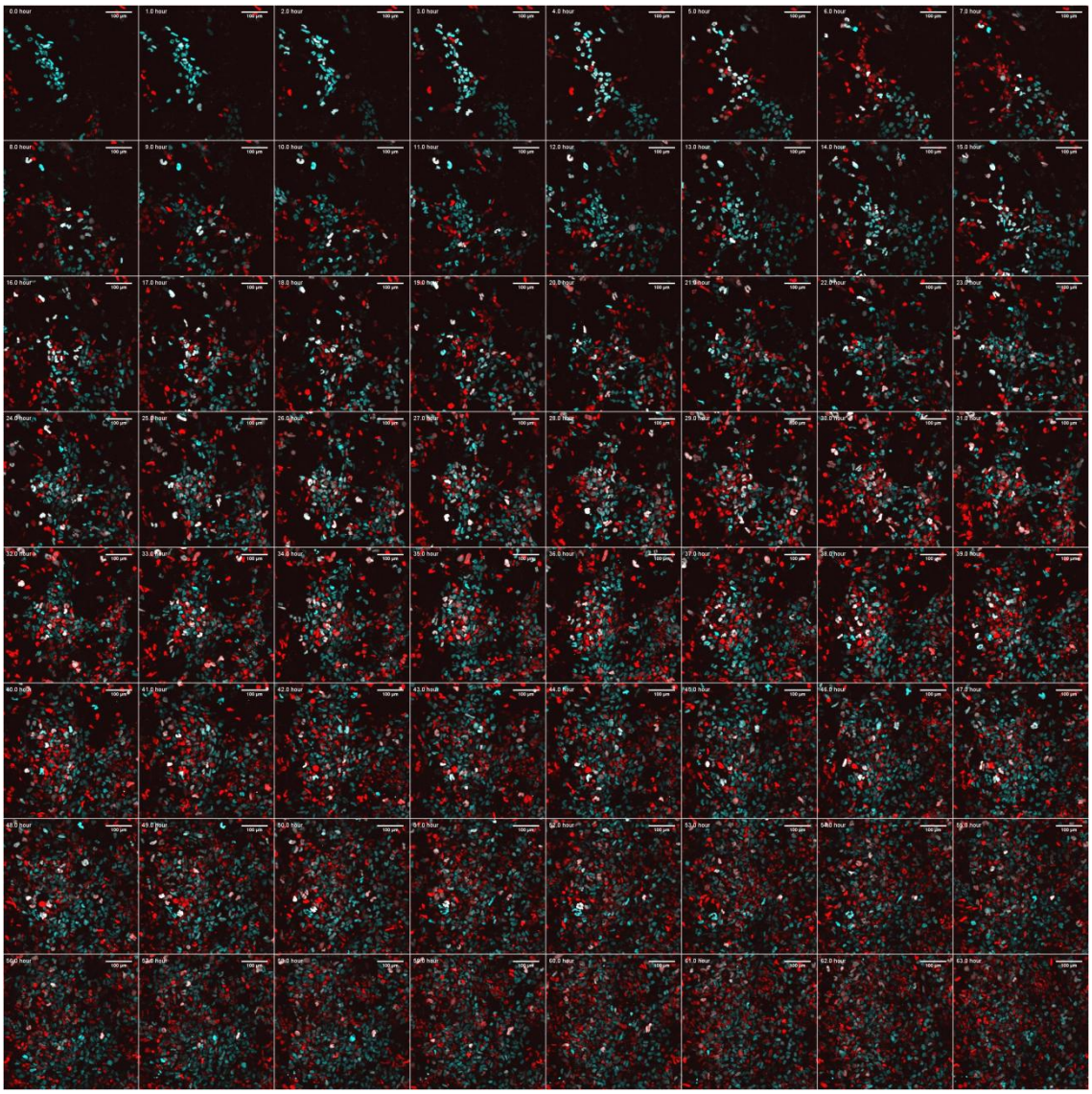

Figure 2-11. Time-lapse imaging of riPSCs using Fucci4 probes. Time-lapse imaging was performed by FV1000-D for 63 hours. Since Fucci4 was used in this imaging, the combinations of fluorescence color and phases of cell cycle are G_1-red, S-blue, G_2/M-red and blue (the color of G_2/M is processed to white).

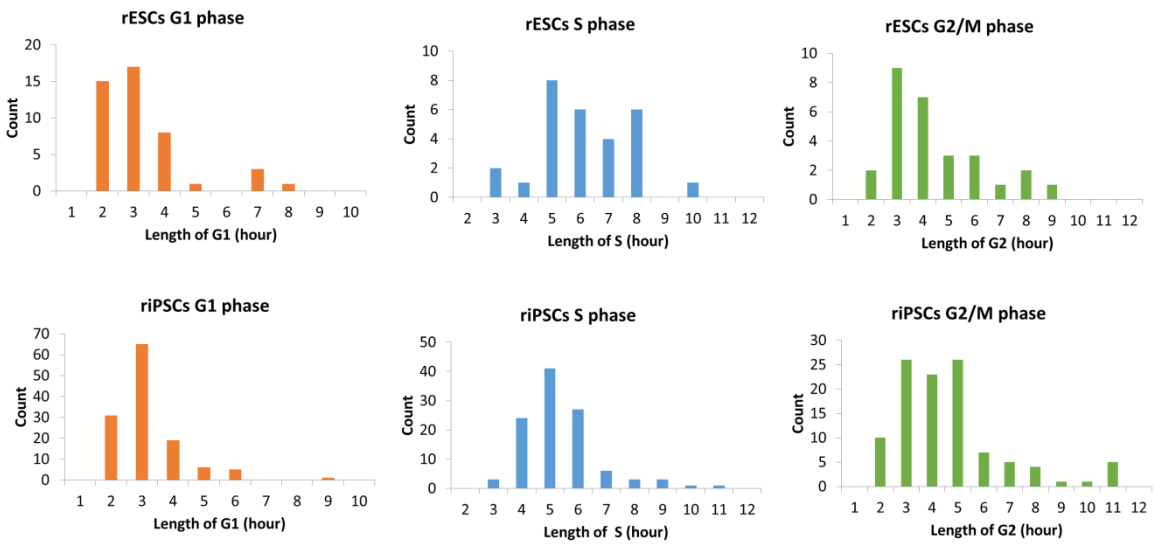

Figure 2-12. The length of each cell cycle phase in individual rabbit PSCs. Each line of three graphs is showing distribution of length of G_1, S, and G_2/M phase. The length of the G_1 length of most rESCs and riPSCs is 2-4 hours, but a significant number of cells have a prolonged G_1 phase more than 5 hours.

(a)

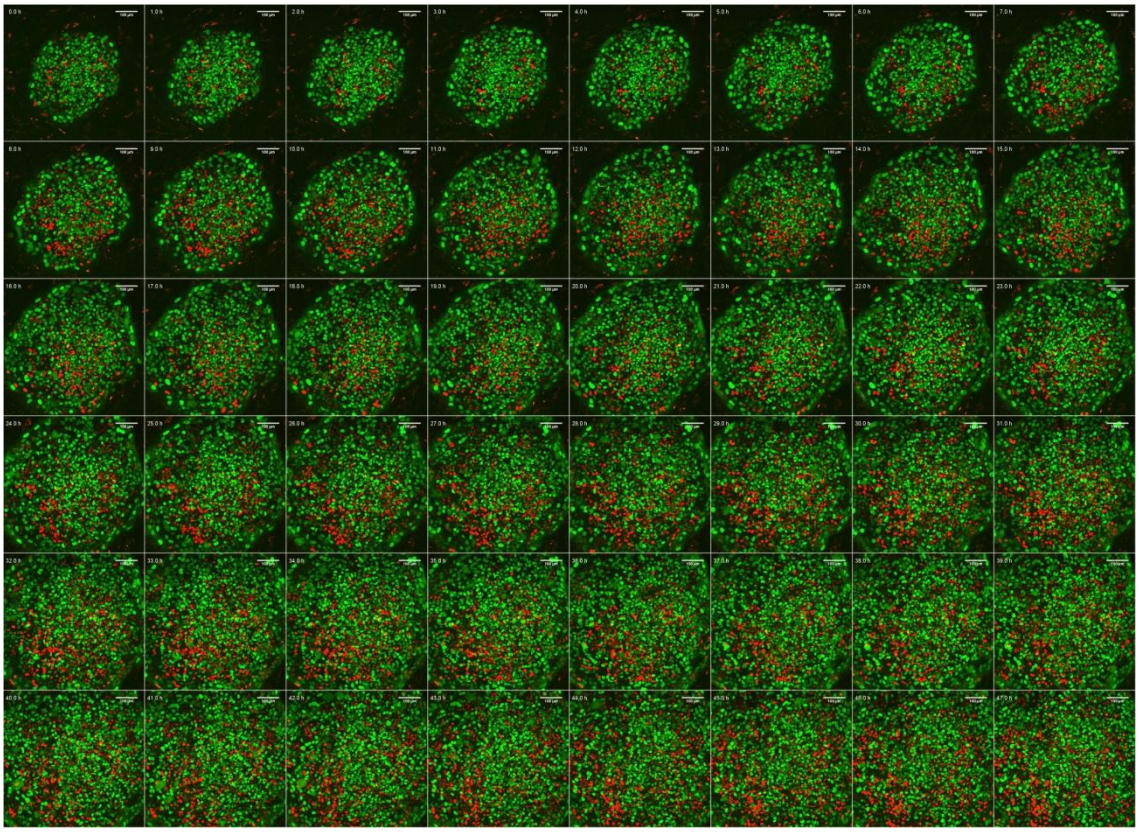

(b)

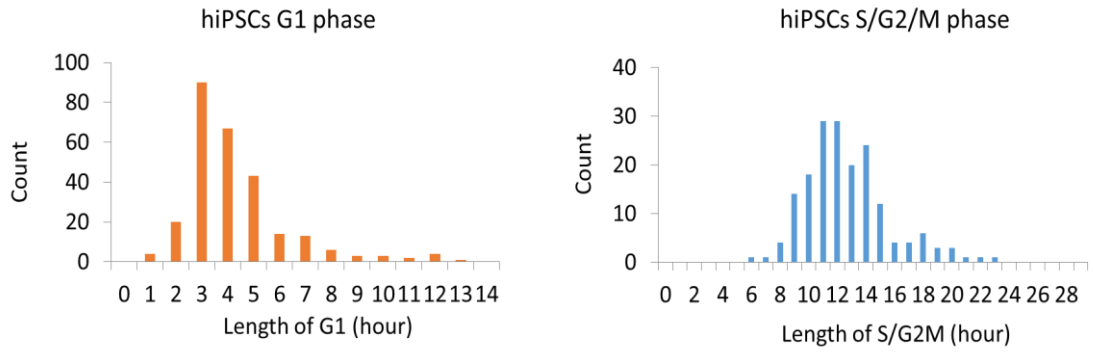

Figure 2-13. Time-lapse imaging of hiPSCs using Fucci2 probes. (a) Time-lapse imaging was performed with an FV1000-D for 49 hours. Since Fucci2 was used in this imaging, the combinations of fluorescence color and phases of cell cycle are G_1-red, S/G_2/M-green, G_1/S-red and green (the color of G_1/S is processed to yellow). (b) The length of each cell cycle phase in individual hiPSCs.

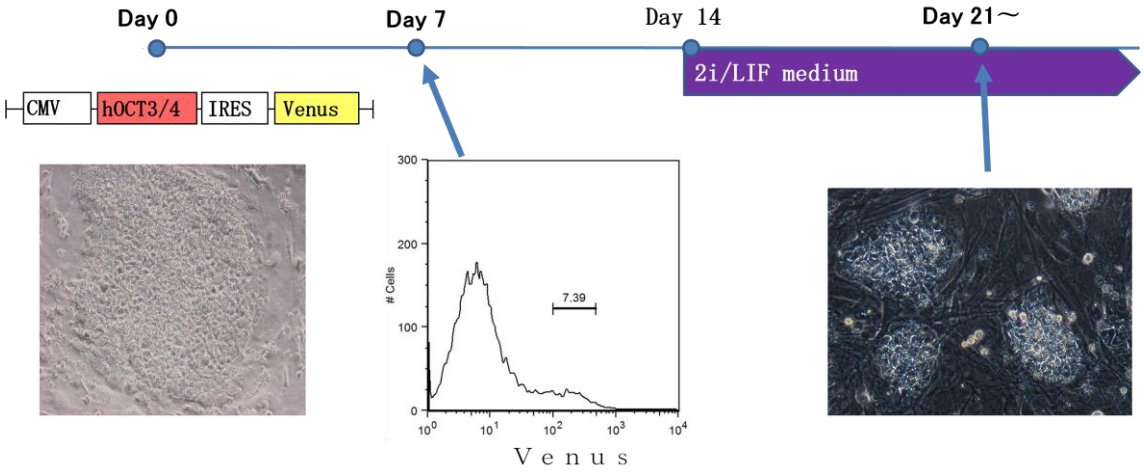

Figure 2-14. Generating naïve-like hiPSCs. hiPSCs were transduced with the lentiviral vector expressing hOCT3/4-IRES-Venus. About one week after, Venus-positive cells were isolated and cultured about one week in primed PSCs medium. After colony formation, culture medium was replaced by naïve medium contained forskolin, and naïve PSCs-like colonies were picked up.

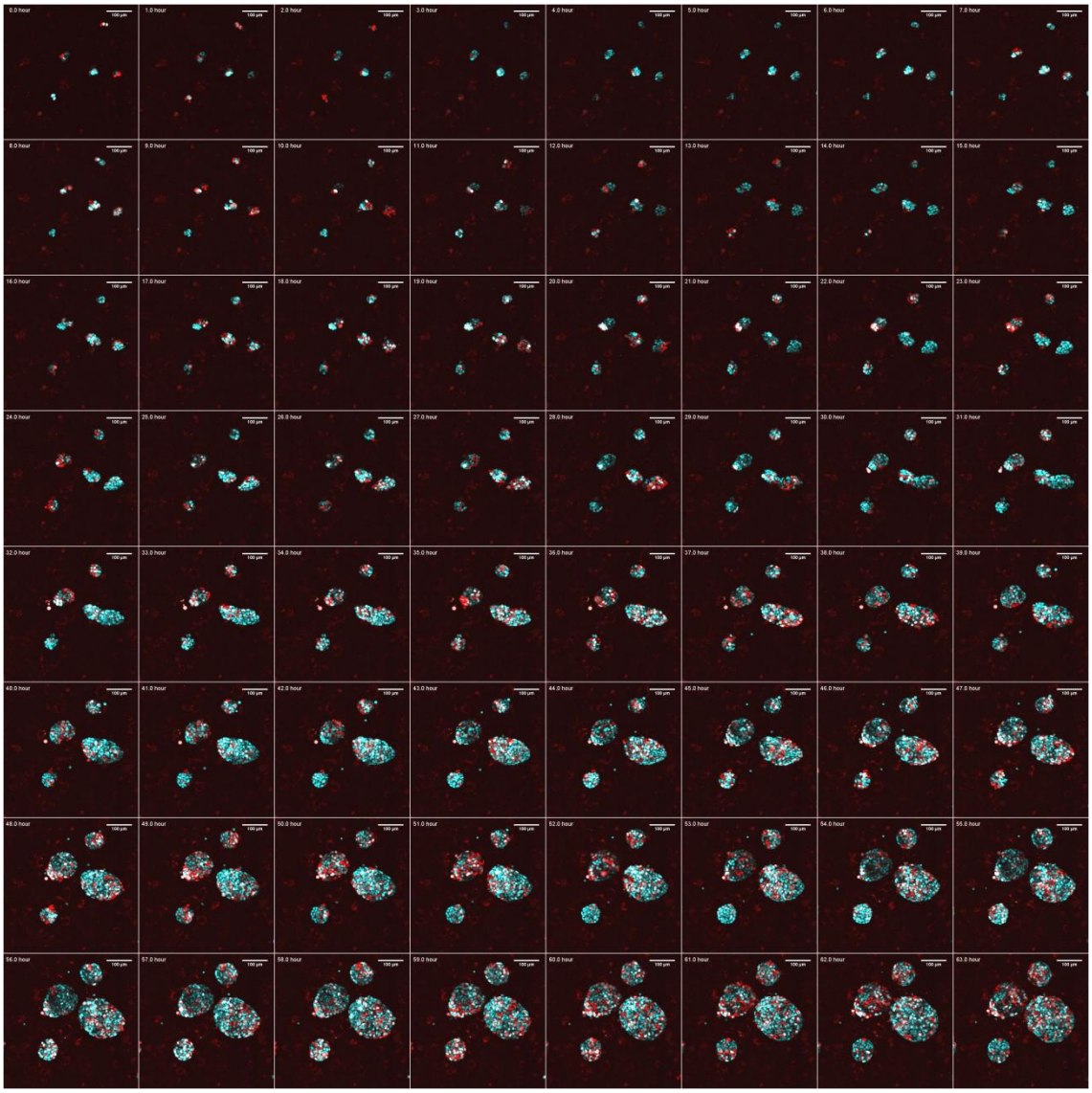

Figure 2-15. Time-lapse imaging of naïve-like riPSCs using Fucci4 probes. Time-lapse imaging was performed with FV1000-D for 63 hours. Since Fucci4 was used in this imaging, the combinations of fluorescence color and phases of cell cycle are G_1-red, S-blue, G_2/M-red and blue (the color of G_2/M is processed to white).

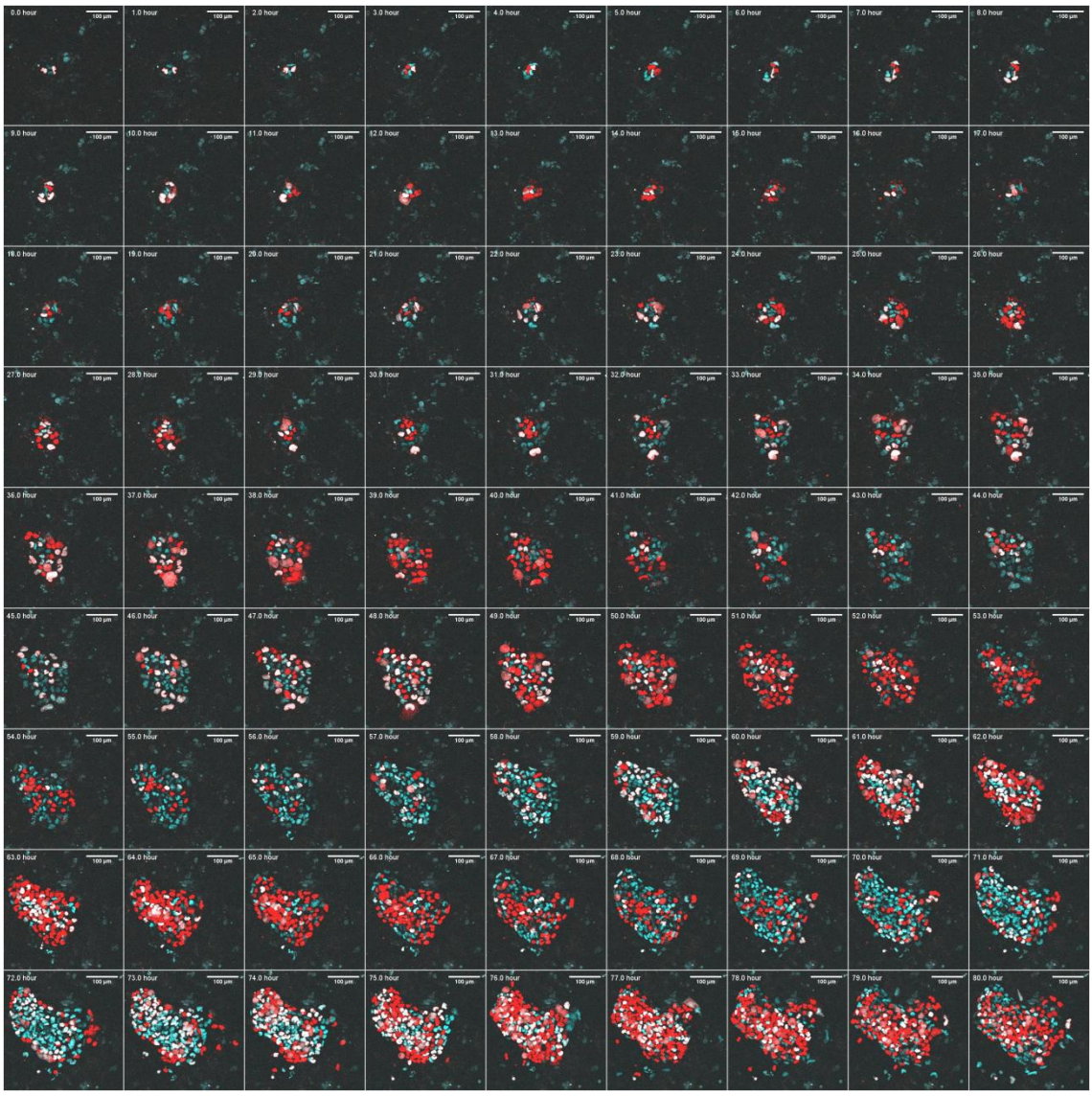

Figure 2-16. Time-lapse imaging of naïve-like hiPSCs using Fucci4 probes. Time-lapse imaging was performed with FV1000-D for 80 hours. Since Fucci4 was used in this imaging, the combinations of fluorescence color and phases of cell cycle are G_1-red, S-blue, G_2/M-red and blue (the color of G_2/M is processed to white).

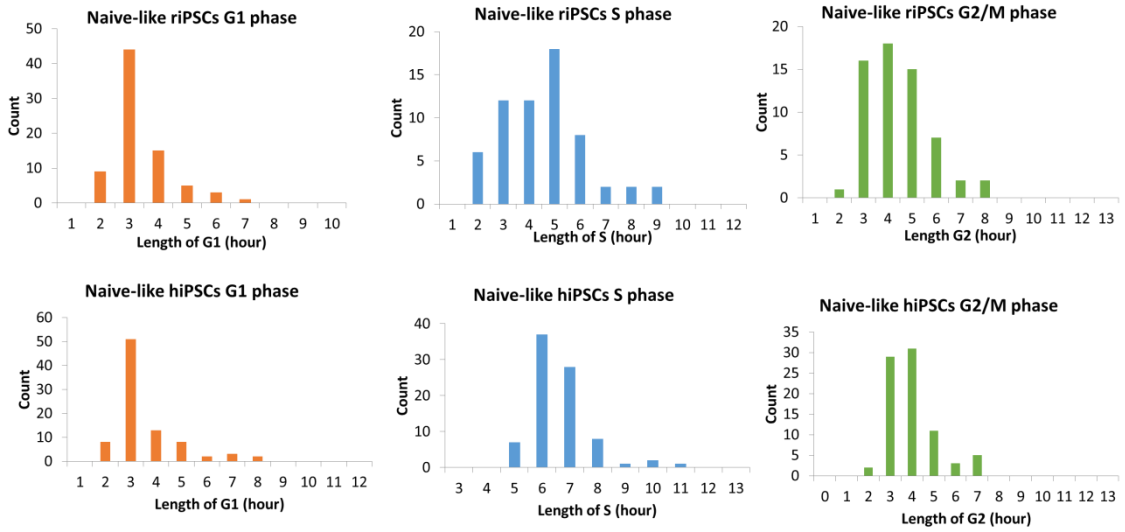

Figure 2-17. The length of each cell cycle phase in individual naïve-like PSCs. Each line of three graphs is showing distribution of length of G_1, S, and G_2/M phase. The mean length of the G_1 phase of naïve-like hiPSCs and naïve-like riPSCs is shorter than corresponding primed iPSCs, but cells with prolonged G_1 phase longer than 5 hours are also observed.

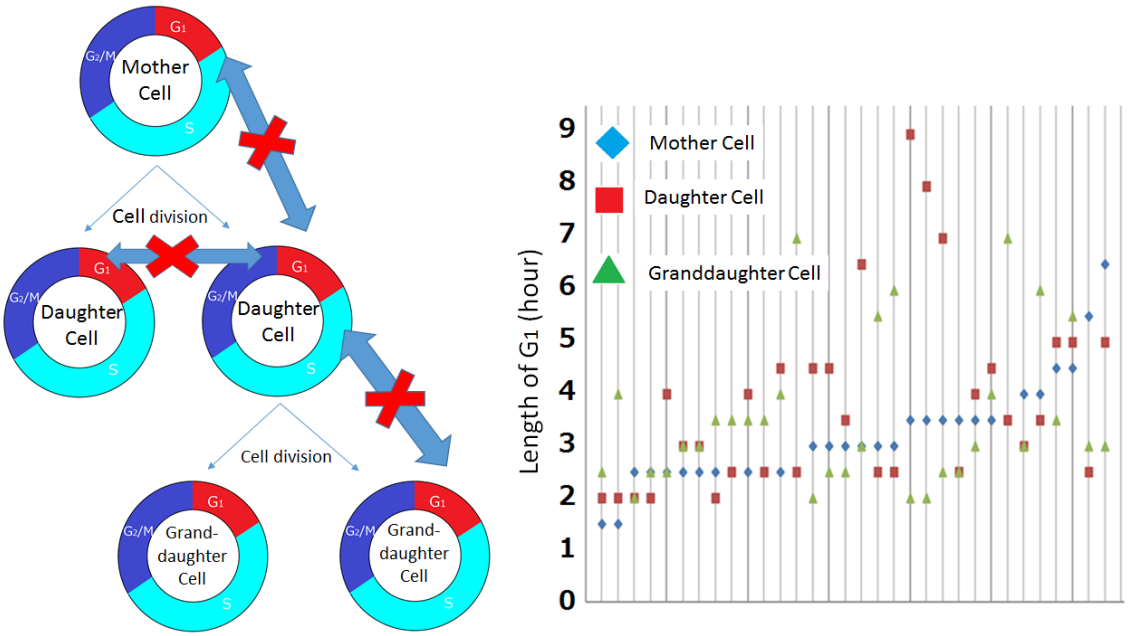

Figure 2-18. Comparison of the G_1 phase length in sequential cell division. X-axis shows sequential cell division of individual cells. Y-axis shows the length of each G_1 phase.

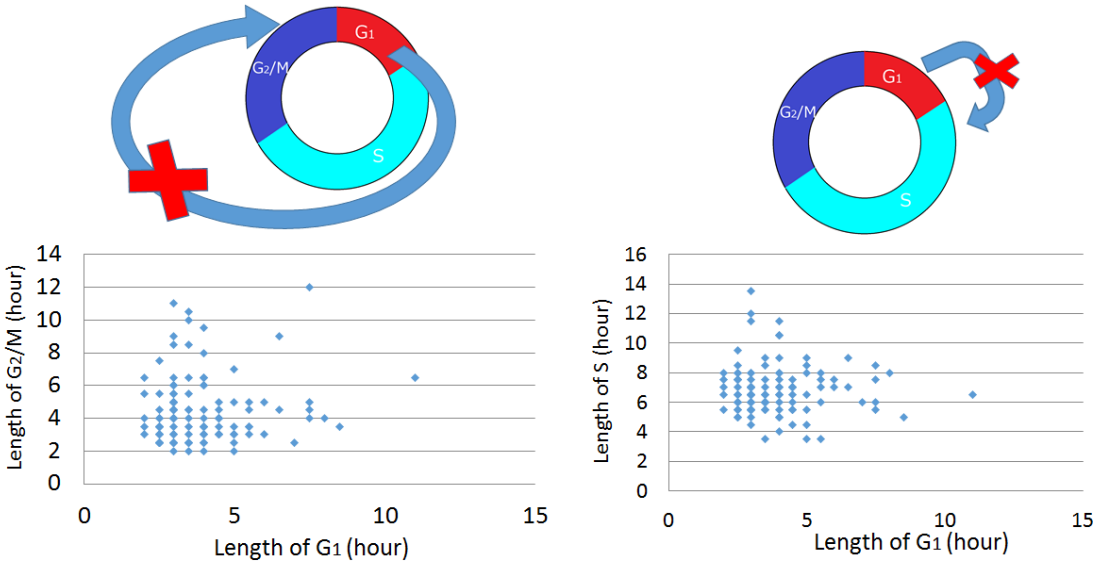

Figure 2-19. Comparison of the length of the G_1 phase and S/G_2/M phases in individual cells. (a) Relationship between G_1 phase and G2/M phases. (b) Relationship between G_1 phase and S phase.

(a) (b)

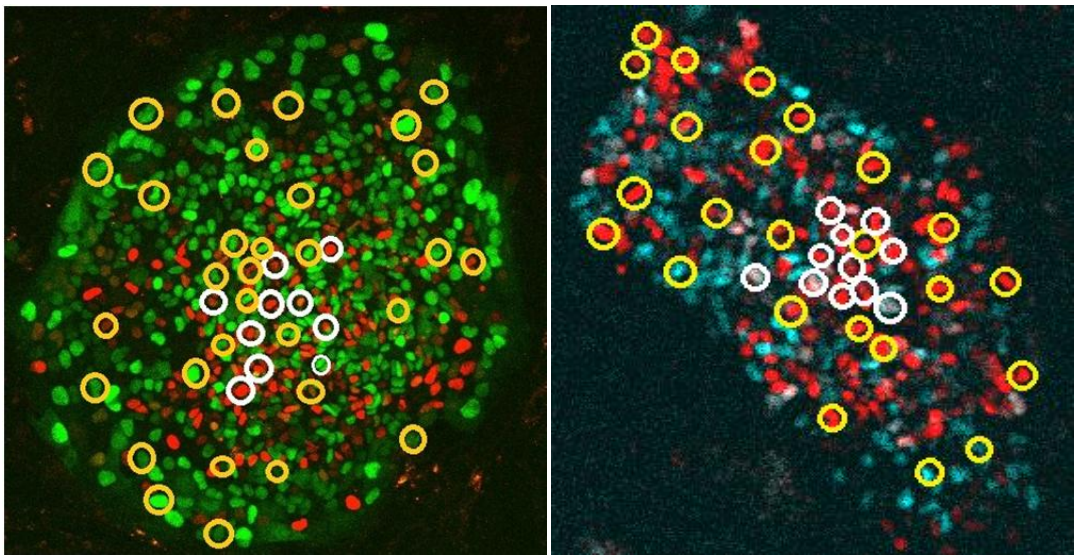

Figure 2-20. Spatio-ununiformity of cell cycle in the conoly. (a) hiPSCs. (b) mEpiSCs. Yellow circles show the position of hiPSCs that have a short G_1 phase. White circles show the position of hiPSCs that have a prolonged G_1 phase.

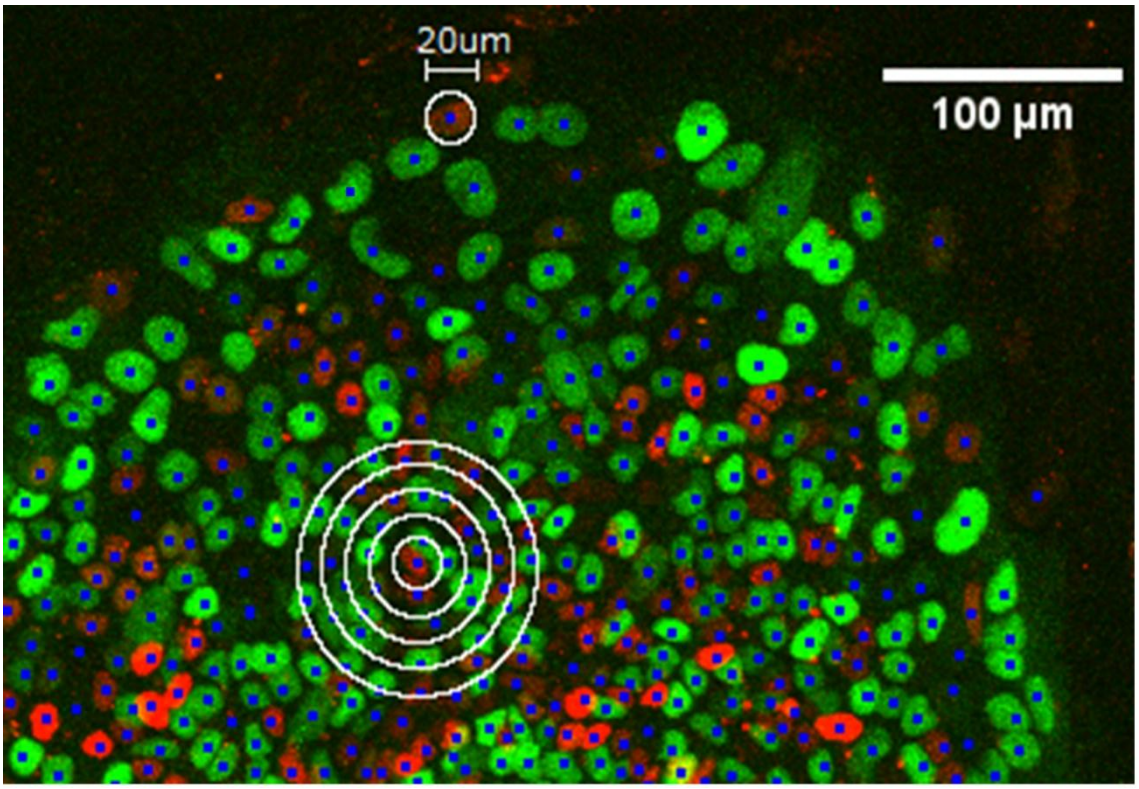

Figure 2-21. Definition of cell density. The cell density is defined as the number of cells within a circle with 20, 30, or 40 µm diameter from a selected cell in each time-lapse frame

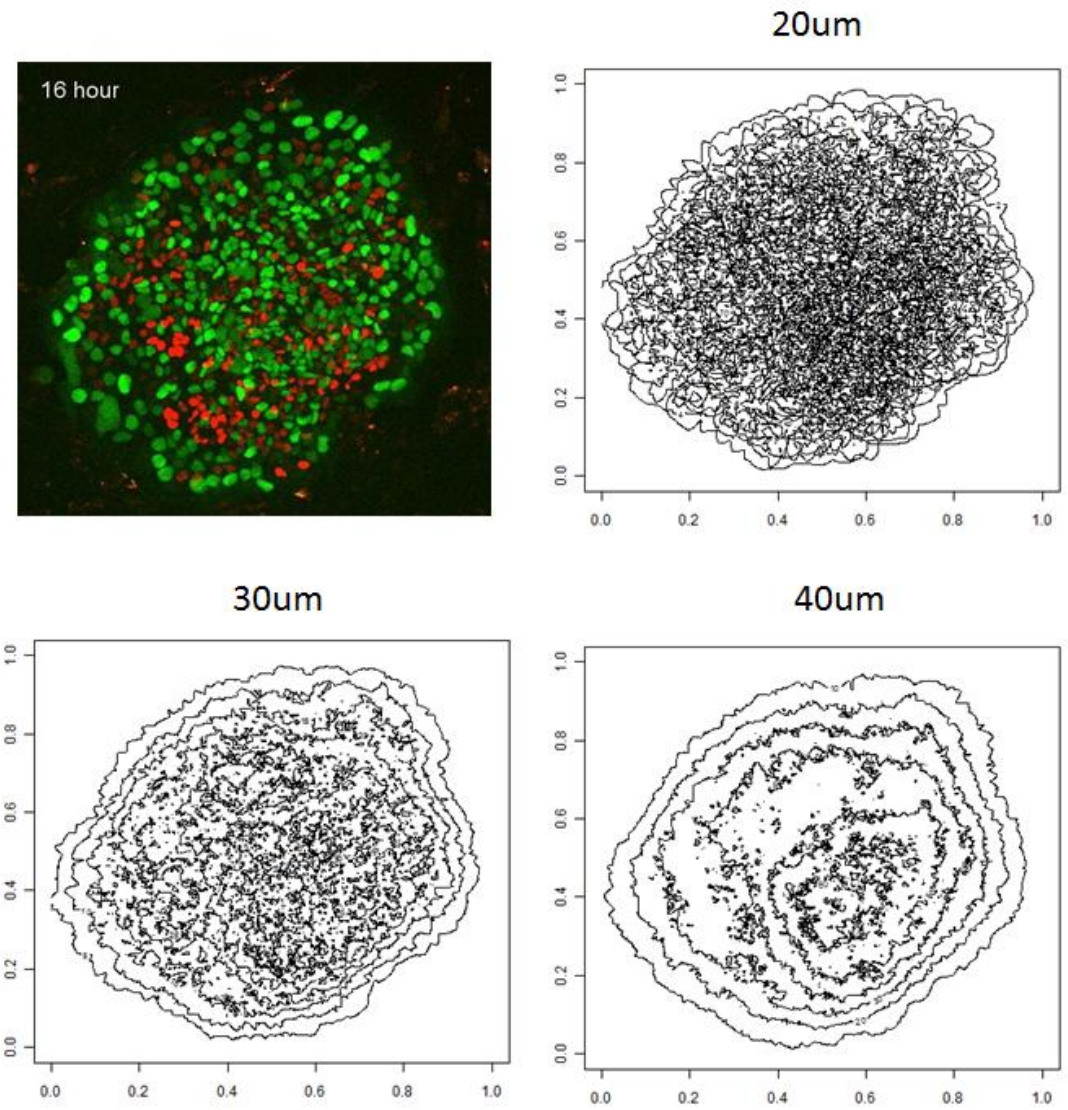

Figure 2-22. The contour map of hiPSC colony. The contour maps show the number of cells within 20, 30, or 40 μm diameter from all selected cells. As compared with the original image, the cell density is measured correctively.

(a)

Phase	M	M/d	G1	G1	G1	G1	S/G2	S/G2	S/G2	S/G2	M	M/d
Cell count	8	9	10	11	12	13	12	14	15	15	16	16

Average 11.5 Average 14.7

(b)

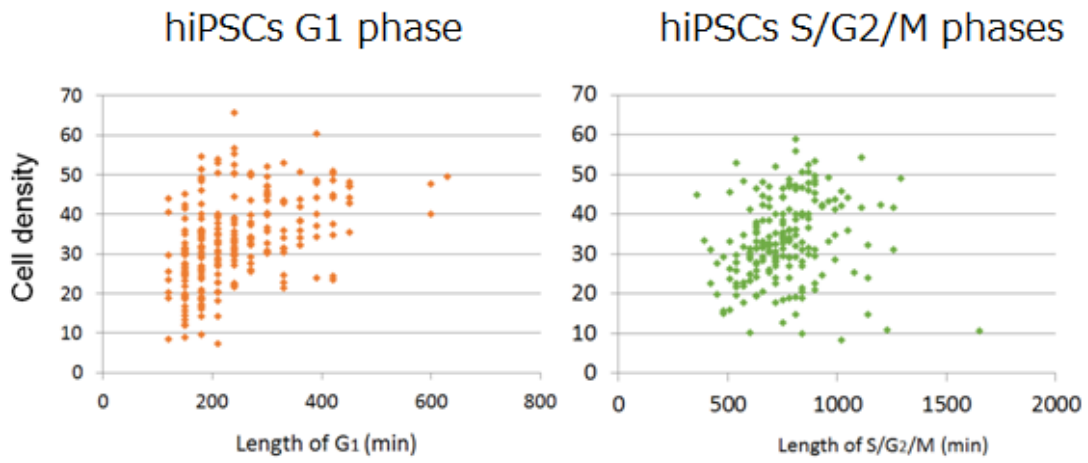

Figure 2-23. Correlation between the length of each cell cycle phase and the cell density. The cell density was calculated as an average of cell count during G_1 or S/G_2/M phases in each time-laps frame. (a) Correlation between the length of the G_1 phase and the cell density. (b) Correlation between the length of the S/G_2/M phases and the cell density.

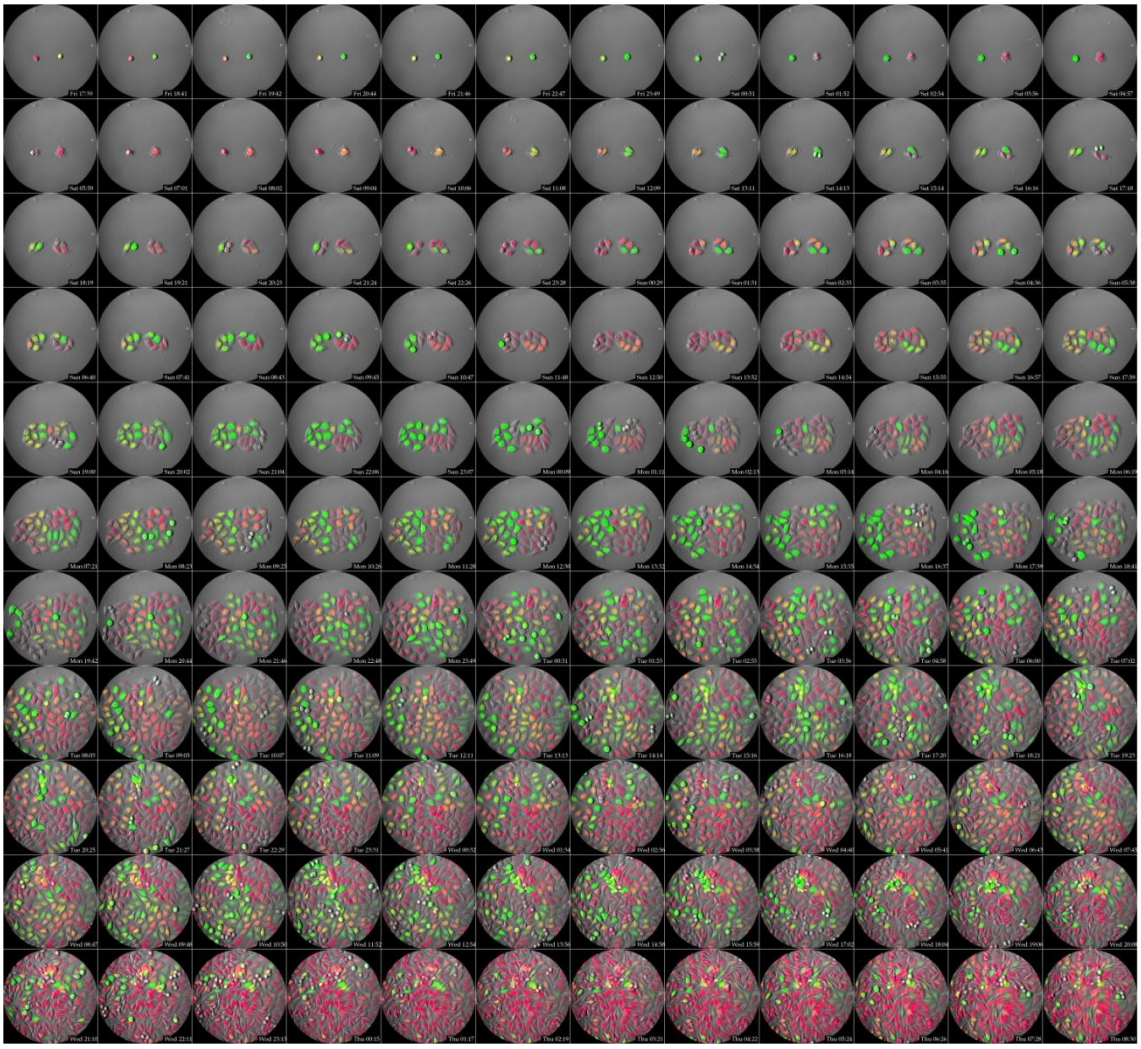

Figure 2-24. Time-lapse imaging of HeLa cells using Fucci2 probes. Time-lapse imaging was performed with an LCV110 for 132 hours. Since Fucci2 was used in this imaging, the combinations of fluorescence color and phases of cell cycle are G_1- red, S/G2/M-green, G_1/S-red and green (the color of G_1/S is processed to yellow).

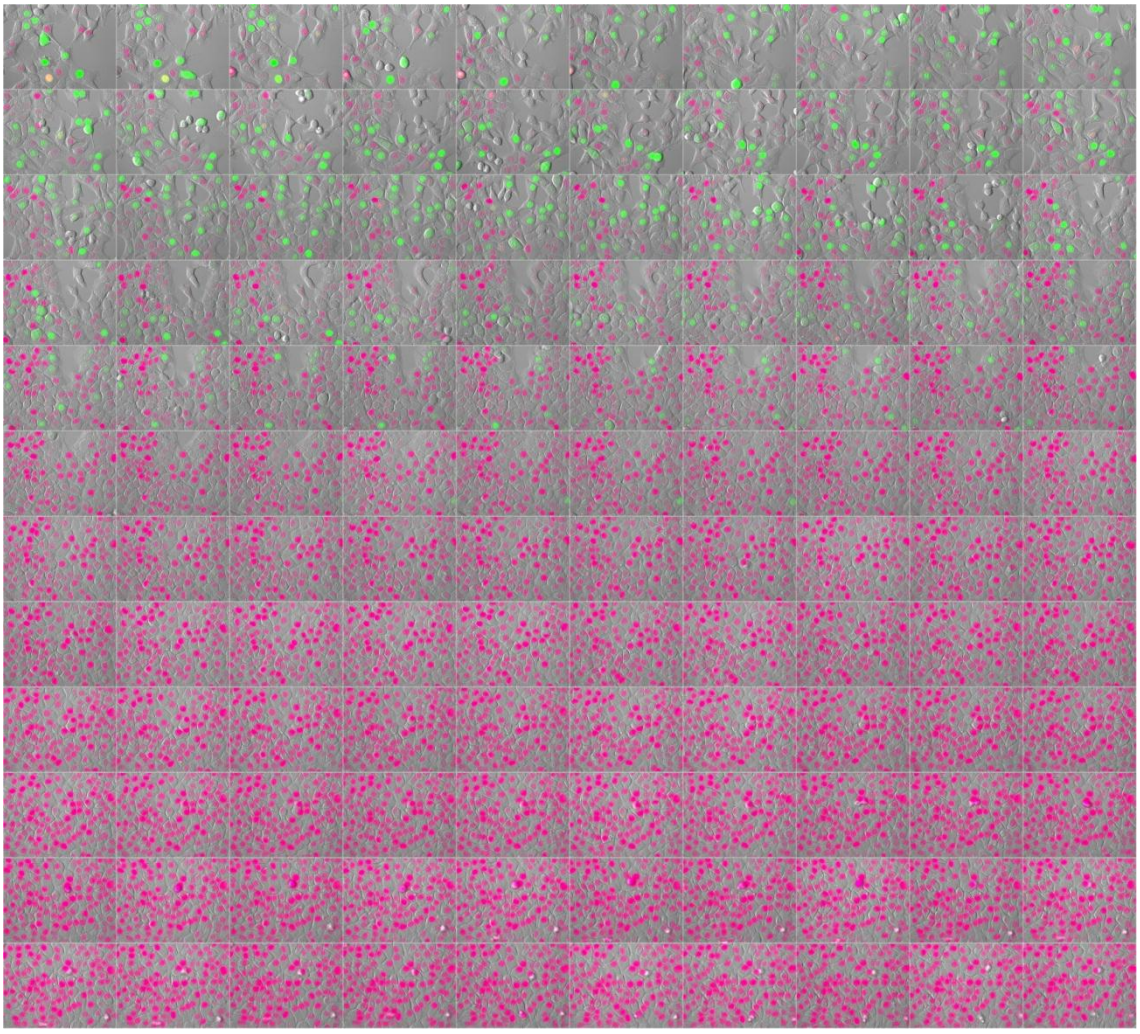

Figure 2-25. Time-lapse imaging of NMuMG cells using Fucci2 probes. Time-lapse imaging was performed with an LCV110 for 120 hours. Since Fucci2 was used in this imaging, the combinations of fluorescence color and phases of cell cycle are G_1- red, S/G_2/M-green, G_1/S-red and green (the color of G_1/S is processed to yellow).

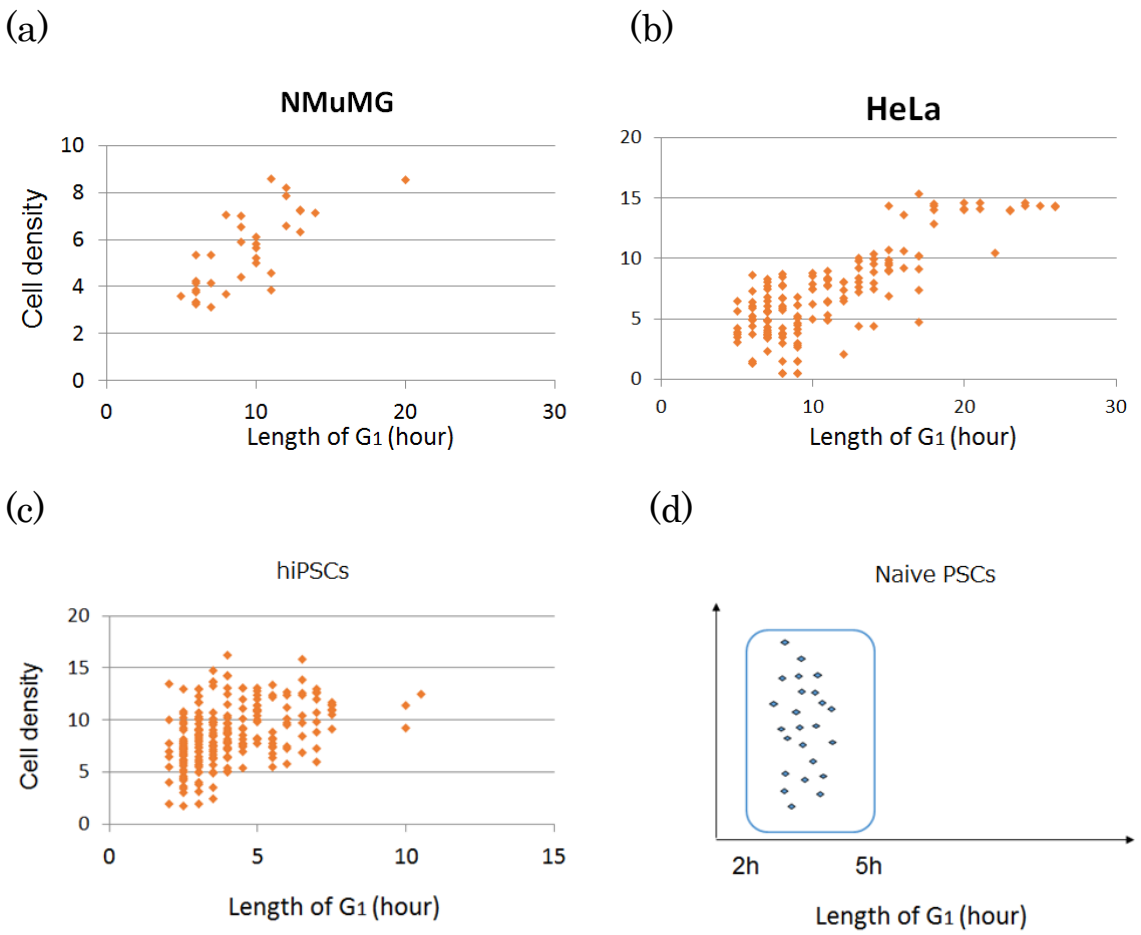

Figure 2-26. Correlation between the G1 phase length and the cell density. (a)–(b) HeLa and NMuMG cells are affected by contact inhibition. The G1 phase length increased in direct proportion to the cell density (c) In case of iPS cells, if iPS cells were affected contact inhibition, length of G1 delay is at random, minimum delay is no delay, maximum delay is not beyond border which is in proportion to cell density. (d) Cell density of naïve PSCs cannot be measured for steric colony formation, but G1 phase dynamics of mESCs/iPSCs are predicted to ignore the cell density

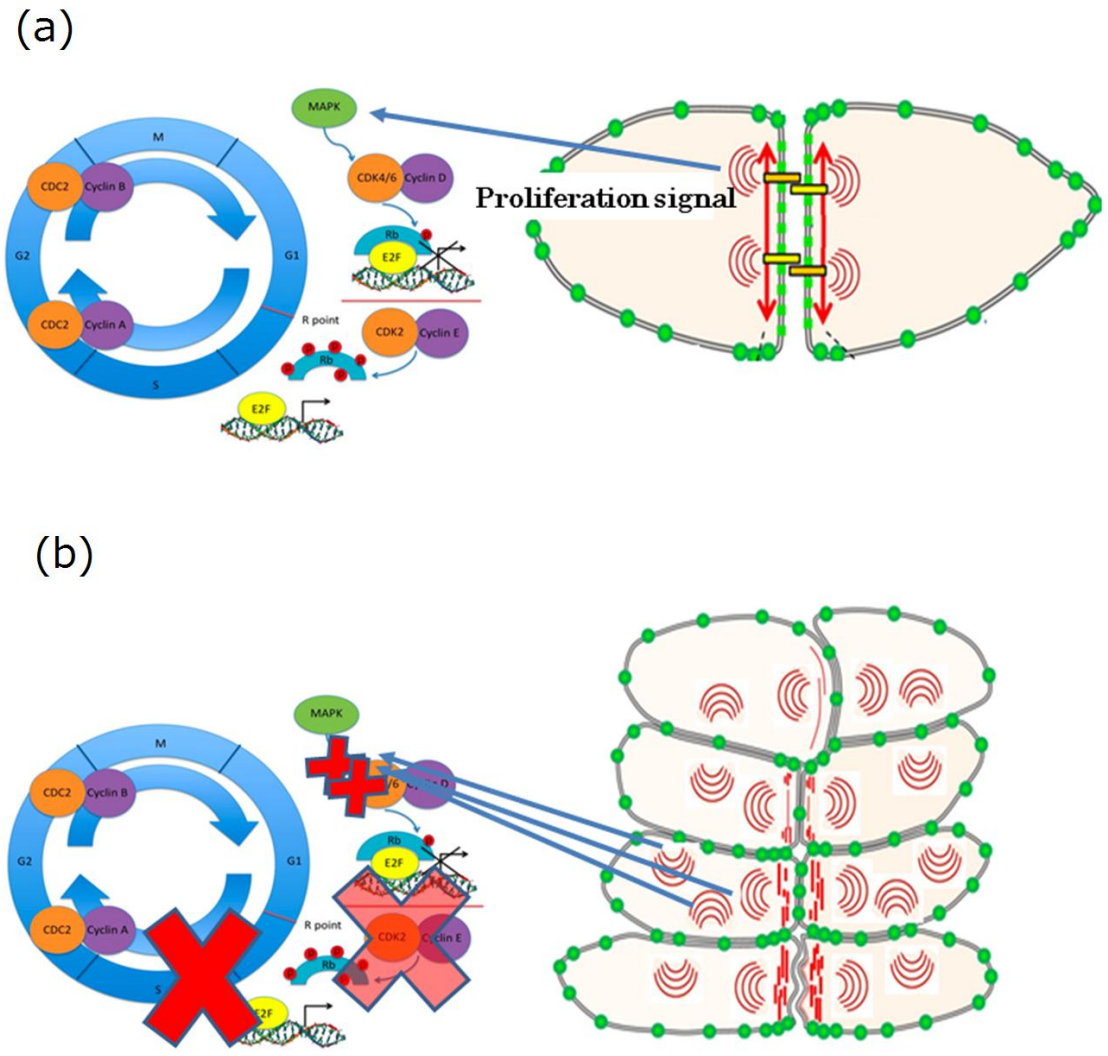

Modified Fagotto F et al. (2013) and Symonds CE et al. (2009)

Figure 2-27. The mechanism of contact inhibition in differentiated somatic cells. (a) In differentiated somatic cells, when cells contacted other cells, proliferation signals are transmitted and the cell cycle is progressed by activation of cell cycle pathway. (b) Excessive proliferation signals arrest cells in G_1 phase or enter cells in quiescent G_0 phase.

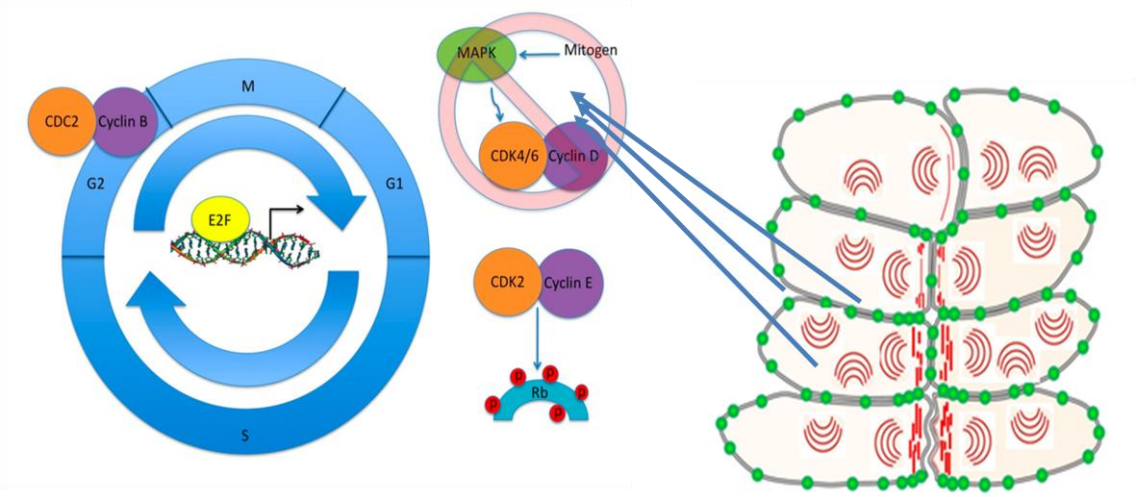

Modified Fagotto F et al. (2013) and Symonds CE et al. (2009)

Figure 2-28. Cell cycle mechanism of mESCs. Cell cycle progression of mESCs is stimulated by autocrine loop of proliferation signaling and does not require exogenous growth factors.

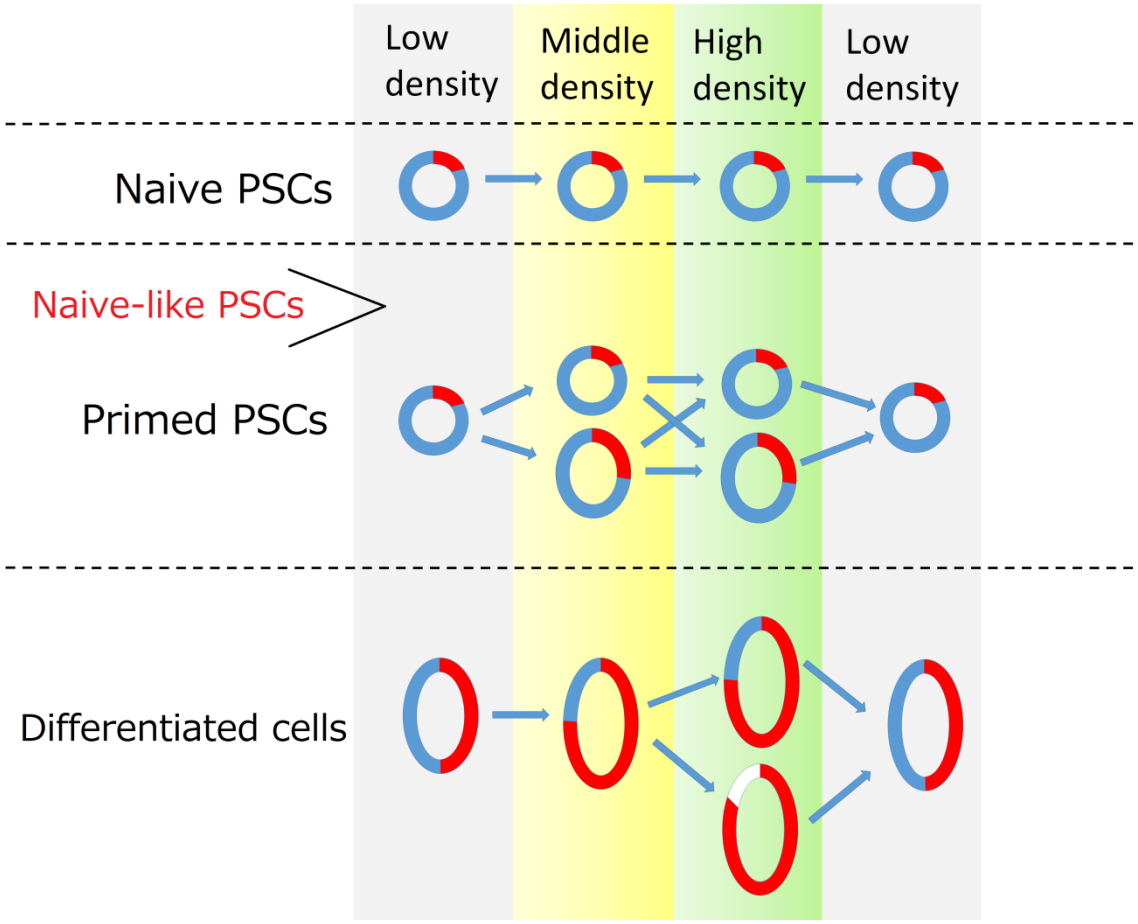

Figure 2-29. Correlation between the G1 phase length and the cell density. Naïve PSCs are not subject to contact inhibition. On the other hand, differentiated somatic cells are affected by contact inhibition, resulting in cell cycle arrest. In primed PSCs and probably naïve-like PSCs, the length of the G1 phase is affected by contact inhibition.

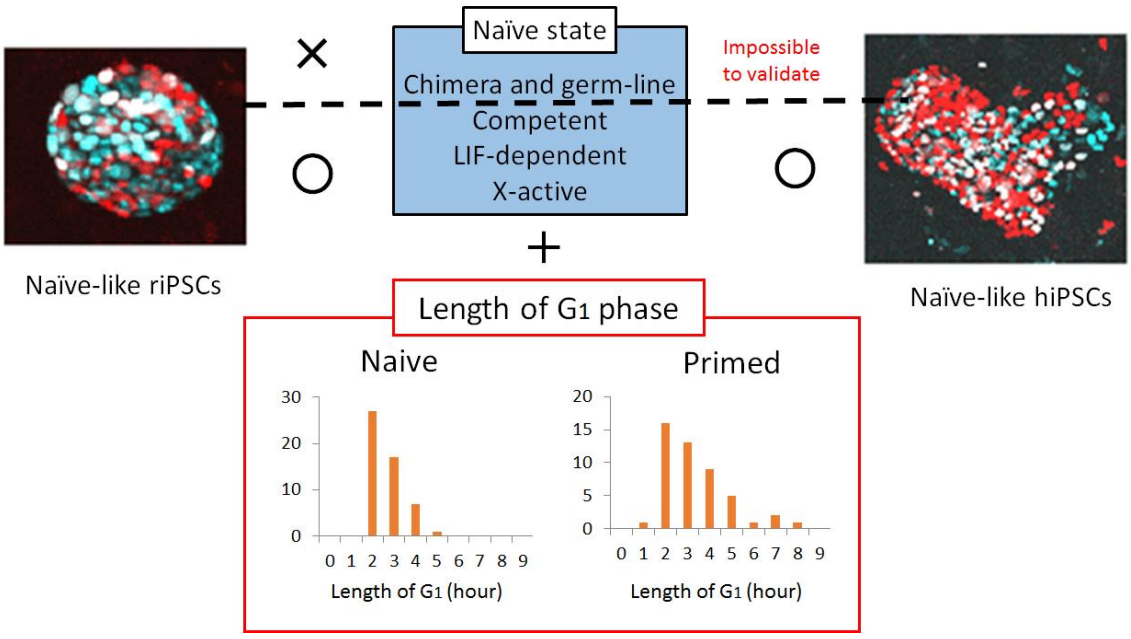

Figure 2-30. Novel feature of Naïve PSCs. The results in this study suggest that a short G_1 phase that is not affected by the cell density can be a novel feature of naïve state.

Table 1. The mean length of the cell cycle stages in mouse, rabbit, and human PSCs.

Cell types	Length of the cell cycle stages (mean±SD)		
	G_1 phase (hour)	S phase (hour)	G_2/M phase (hour)
mESCs	2.41±0.79	5.67±1.27	3.60±1.31
miPSCs	2.35±0.74	5.08±1.81	3.10±1.00
mEpiSCs	3.03±1.45	4.96±1.36	3.23±1.12
rESCs	3.02±0.75	5.84±1.65	4.09±2.14
riPSCs	2.93±1.28	5.10±1.40	4.53±2.36
Naïve-like riPSCs	3.26±0.81	6.77±0.82	3.41±1.30
hESCs	3.50±1.09	6.48±1.10	4.24±1.54
hiPSCs	4.31±1.85	7.22±2.10	4.75±2.50
Naïve-like hiPSCs	3.31±1.29	6.34±1.03	3.85±1.56